JOURNAL OF GUIDANCE, CONTROL, AND DYNAMICS
Vol. 40, No. 8, August 2017

Magnetic Attitude Control with Impulsive Thrusting Using the Hybrid Passivity Theorem

Behrad Vatankhahghadim* and Christopher J. Damaren†
University of Toronto, Toronto, Ontario M3H 5T6, Canada

DOI: 10.2514/1.G002375

Passivity-based design approaches for hybrid attitude control of spacecraft using continuous magnetic torques and impulsive thrusts are proposed. The classical passivity notions, the passivity theorem, and the Kalman–Yakubovich–Popov conditions are extended to hybrid systems and used for linear passivity-based controller design. The plant's output dynamics are manipulated such that the hybrid extended (time-varying) Kalman–Yakubovich–Popov conditions are satisfied, hence establishing the plant's passivity. Then, evoking the hybrid passivity theorem that states the negative feedback interconnection of a passive hybrid plant and an input strictly passive hybrid controller is input–output stable, two such controllers are proposed: a proportional feedback controller with constant positive gains; and a dynamic compensator, developed using the hybrid algebraic (time-invariant) Kalman–Yakubovich–Popov conditions, that actively adjusts the gains based on the system's dynamics and response. Numerical simulations validate the proposed controllers' functionality and suggest performance improvements gained via hybrid control. The effects of random sensor noise are also studied, and the results suggest enhanced immunity in terms of performance arising from the use of the dynamic compensator instead of the constant-gain controller.

Nomenclature

A	=	magnetic torquer cross section, m^2
a	=	semimajor axis, m
$\boldsymbol{b}$	=	magnetic field vector, T
$\boldsymbol{C}$	=	rotation matrix between two frames
c	=	magnetic torquer turns per coil
d	=	magnetic torquer coil side length, m
E	=	magnetic torquer energy usage, MJ
$\boldsymbol{E}$	=	matrix of eigenvectors (as columns)
e	=	eccentricity
$\boldsymbol{I}$	=	moment of inertia matrix, kg $\cdot$ m^2
i	=	inclination, rad
$\boldsymbol{m}$	=	magnetic dipole moments, A $\cdot$ m^2
N	=	total number of impulses (plus one)
$\mathbb{N}$	=	natural numbers (positive integers)
$\hat{N}$	=	pretruncation impulses (plus one)
$\boldsymbol{n}$	=	impulsive thrust gains, N $\cdot$ m
n	=	number of impulses per orbit (plus one)
$\boldsymbol{P}$	=	Lyapunov solution
R	=	magnetic torquer coil resistance, Ω
$\mathbb{R}$	=	real numbers
$\mathbb{R}^+$	=	nonnegative real numbers
$\boldsymbol{r}$	=	position vector, m
T	=	orbital period, s
t_0	=	time of perigee passage, s
$\hat{t}$	=	truncation time, s
V	=	storage function
$\mathbb{W}$	=	whole numbers ($\mathbb{N} \cup \{0\}$)
$\delta(t)$	=	Dirac delta function
$\boldsymbol{\Sigma}$	=	noise covariance matrix
$\boldsymbol{\epsilon}$	=	vector part of quaternions
η	=	scalar part of quaternions
$\boldsymbol{\theta}$	=	attitude Euler angles, rad
$\boldsymbol{\Lambda}$	=	matrix of eigenvalues (as diagonals)
μ	=	gravitational parameter, m^3/s^2
ρ	=	vector of random numbers
σ	=	noise variance
$\boldsymbol{\tau}$	=	torque vector, N $\cdot$ m
ϕ	=	angle from Euler axis angle, rad
Ω	=	longitude of ascending node, rad
$\boldsymbol{\omega}$	=	angular velocity vector, rad/s
ω	=	argument of periapsis, rad
$\mathbf{0}_{m\times n}$	=	$m \times n$ zero matrix
$\mathbf{1}_{n\times n}$	=	$n \times n$ identity matrix
$\dot{(\cdot)}$	=	differentiation with respect to time
$\lvert\cdot\rvert$	=	Euclidean norm of a vector
$\lVert\cdot\rVert$	=	root mean square norm of a quantity
$\lVert\cdot\rVert_p$	=	p norm of a quantity
$(\cdot)^\times$	=	skew-symmetric matrix operator
$\bar{(\cdot)}$	=	averaged or steady-state value

Subscripts

B	=	in body-fixed frame
c	=	continuous-time
d	=	discrete-time
dist	=	disturbance
e	=	extended
f	=	final value
G	=	in Earth-centered inertial frame
nT	=	computed over n orbital periods
nz	=	nonzero
$\hat{t}$	=	truncated at $\hat{t}$
z	=	zero
0	=	initial value

Superscripts

$(\cdot)^h$	=	hybrid
$(\cdot)^+$	=	postimpulse quantity
$(\cdot)^-$	=	preimpulse quantity

Presented as Paper 2017-1738 at the AIAA Guidance, Navigation, and Control Conference, Grapevine, TX, 9–13 January 2017; received 28 July 2016; revision received 6 March 2017; accepted for publication 7 March 2017; published online 25 May 2017.

*Graduate Student, Spacecraft Dynamics and Control Laboratory, Institute for Aerospace Studies, 4925 Dufferin Street. Student Member AIAA.

†Professor and Director, Institute for Aerospace Studies, 4925 Dufferin Street. Associate Fellow AIAA.

I. Introduction

THIS paper focuses on passivity-based control of hybrid (continuous/impulsive) systems, with applications to the hybrid system emerging from combination of magnetic torquers and

impulsive thrusters for spacecraft attitude control purposes. Passivity is intimately tied to the notion of energy and, for the interconnection of a plant and a controller, the passivity theorem (that states the negative feedback of a passive plant and an input strictly passive controller is input–output stable) enables a physical interpretation of stability by considering how much energy is injected into and dissipated by the system [1]. A survey of passivity-based feedback control designs was presented in [2]. Using the positive realness of a system's transfer function for stability analysis and developing algebraic criteria to guarantee this property date back to classical papers such as [3–6]. A discussion of the more generalized concept of dissipativity, of which passivity is a special case, was provided in [7,8], and an extension of dissipativity to affine nonlinear systems was performed in [9]. Extending the notion of dissipativity to nonlinear hybrid systems that also include impulsive dynamics, a rigorous study on the stability of open-loop systems and their feedback interconnection was conducted in [10,11], respectively. Also presented in [10] were generalized interpretations of hybrid energy balance between the system's stored and dissipated energies, as well as a specialization of the stability results and the extended algebraic Kalman–Yakubovich–Popov (KYP) conditions to passive and nonexpansive hybrid systems. A notion of passivity for switched systems with multiple continuous states that are mapped by a set of discrete states (also referred to as "hybrid") was provided in [12].

In terms of applications, passivity-based nonlinear control synthesis was explored in [13], in which a brief discussion of possible extensions to discrete-time systems was also provided. Passification methods (for rendering a system passive) were proposed in [14] for passivity-based design of nonpassive systems, such as some flexible aerospace structures. An example of passive design for hybrid impulsive systems that exhibit dissipation only in continuous- or discrete-time dynamics was considered in [15]. Focusing on spacecraft equipped with magnetic torquers and reaction wheels, passivity-based design was used in [16] for attitude control. Some other spacecraft-related applications of the passivity theorem were discussed in [17].

In this paper, a set of extended KYP conditions similar to those derived in [10] for hybrid impulsive systems, in conjunction with additional extensions to time-varying systems resembling those in [16], is employed to design a plant that is passive, in a hybrid sense. Two different feedback controllers are then considered, which are both input strictly passive, as required by the passivity theorem: a proportional hybrid controller with positive constant gains for both continuous- and discrete-time outputs, and a dynamic compensator (similar to the one proposed in [18]) that judiciously adjusts the feedback gains and ensures the controller's input strict passivity using a hybrid extension of a specialization of the algebraic KYP conditions of [10]. Adopting a passivity-based control scheme is primarily motivated by expectations on the robustness of such controllers [14,16], whereas proposing a dynamic compensator in addition to a simple constant-gain controller is driven by the latter's enhanced capability in filtering out sensor noise and in producing potentially smoother control inputs.

Attitude control using magnetic torquers relies on electromagnetic interactions between mutually perpendicular current-carrying coils and the geomagnetic field and, as a result, is a particularly attractive option for near-Earth spacecraft because of its efficiency and absence of fuel requirements [19]. Among earliest studies on magnetic attitude control was that performed in [20], in which the feasibility of using magnetic torquers for two-axis control of the Orbiting Astronomical Observatory was studied and confirmed using experiments. Another practical application to three-axis stabilization of spacecraft was in the Ørsted satellite mission that was launched in 1999 [21–23]. A very recent application, discussed in [24], was in the design of UPMSat-2, which was a microsatellite scheduled for launch in 2015 that relied only on magnetic torquers and magnetometers with new laws based on modifications of the classical B-dot control (originally proposed in [25], with control inputs proportional to the derivative of the magnetic field vector).

A concise survey of the studies performed on magnetic attitude control was provided in [26]. It is well known that this mechanism inherently suffers from instantaneous underactuation that arises from orthogonality of the magnetic field vector to the control torque; however, owing to the time-varying nature of Earth's magnetic field, the attitude control system of interest possesses, on average, controllability properties (over some time interval) for a range of orbit inclinations [22,26,27]. In addition to the pointwise uncontrollability issue, there is also an intrinsic gain limitation associated with stabilization using magnetic actuators, as demonstrated in [28]. Early works on magnetic attitude control include that in [25], in which B-dot control was proposed upon considering approximate solutions to the nonlinear time-varying problem, as well as that in [27], which employed linear time-invariant (LTI) techniques upon averaging the magnetic field over one orbit. With the aim of using magnetic torquers for momentum dumping, [29] also relied on averaging assumptions. Suggested in [30] were some control allocation techniques for auxiliary magnetic controllers used for oscillation dampening. Local and global three-axis stabilization results using purely magnetic control were derived in [21,23], relying on the quasi-periodic nature of the geomagnetic field.

With the quasi-periodicity assumption, various time-varying magnetic attitude controllers were developed in [22], and optimal periodic control approaches were proposed in [31,32]. A magnetic linear quadratic Gaussian controller was presented in [33] using state estimates for feedback. Considering a discrete-time design problem using magnetic actuators, projection-based optimal output feedback control techniques were introduced in [34]. Abandoning the periodicity assumption, full state feedback using only magnetic actuation was considered in [35] for an almost globally stable solution, but the aforementioned scaling condition restricting the control gains remained. Providing an auxiliary impulsive control mechanism to complement the continuous control of the magnetic torquers is thus partly motivated by a need to alleviate the gain limitation inherent to linear magnetic control. Although nonlinear controllers may be able to overcome such a gain limitation associated with proportional-derivative (PD) control, the proposed designs aim to achieve infinite gain margin using linear passivity-based control. Hybrid magnetic attitude control using both continuous and impulsive torques, along with a corresponding hybrid stability analysis approach, were proposed in [36] but, similar to many other previous works, used optimal control concepts (that did not inherently guarantee robustness) as opposed to the passivity-based techniques used in this paper. Passivity-based linear time-varying (LTV) attitude control was addressed in [16], but using reaction wheels (that also provide continuous torques) in tandem with magnetic torquers. This paper focuses on passive continuous/impulsive (referred to as hybrid) attitude control, presenting novel design schemes that are inherently stable owing to their passivity-based design.

The paper's organization is as follows: First, some well-known definitions and lemmas pertaining to passivity, as well as the passivity theorem, are extended in Sec. II to hybrid systems. Sets of hybrid extended and algebraic KYP conditions that apply to time-varying and time-invariant hybrid systems, respectively, are also provided in this section. The kinematics and dynamics of the attitude control problem of interest, in the presence of gravity gradient and residual magnetic disturbance torques, are described in Sec. III. The system model is then linearized in Sec. IV, and the hybrid passivity theorem and KYP conditions of Sec. II are subsequently employed to design two types of passivity-based hybrid magnetic attitude controller: one with constant gains, and one with a dynamic compensator structure. Lastly, some simulation results, using the full nonlinear model, are presented in Sec. V to assess the performance of the proposed control schemes and study the effects of sensor noise on the controllers' performance, and some concluding remarks are provided in Sec. VI.

II. Hybrid Passivity

Consider a hybrid (continuous/impulsive) LTV system, with impulses applied at t_k, $k \in \mathbb{N}$, represented by $\boldsymbol{y} = \mathcal{G}^h \boldsymbol{u}$, where

$\boldsymbol{u} = \{\boldsymbol{u}_c(t), \boldsymbol{u}_{dk}\}$ consists of both continuous- and discrete-time control inputs; and $\boldsymbol{y} = \{\boldsymbol{y}_c(t), \boldsymbol{y}_{dk}\}$ consists of both continuous- and discrete-time outputs. Assume $\boldsymbol{u}_c$ and $\boldsymbol{y}_c$ have the same dimensions as do $\boldsymbol{u}_d$ and $\boldsymbol{y}_d$.

The continuous-time portion of $\mathcal{G}^h$ at $t \neq t_k$ is given, with the initial condition $\boldsymbol{x}(t_0) = \boldsymbol{x}_0$, by

$$\dot{\boldsymbol{x}}(t) = \boldsymbol{A}_c(t)\boldsymbol{x}(t) + \boldsymbol{B}_c(t)\boldsymbol{u}_c(t) \tag{1a}$$

$$\boldsymbol{y}_c(t) = \boldsymbol{C}_c(t)\boldsymbol{x}(t) + \boldsymbol{D}_c(t)\boldsymbol{u}_c(t) \tag{1b}$$

whereas the discrete-time portion of $\mathcal{G}^h$ at $t = t_k$ is given by

$$\boldsymbol{x}(t_k^+) = \boldsymbol{A}_{dk}\boldsymbol{x}(t_k^-) + \boldsymbol{B}_{dk}\boldsymbol{u}_{dk} \tag{2a}$$

$$\boldsymbol{y}_{dk} = \boldsymbol{C}_{dk}\boldsymbol{x}(t_k^-) + \boldsymbol{D}_{dk}\boldsymbol{u}_{dk} \tag{2b}$$

where $\boldsymbol{x}(t)$:$\mathbb{R}^+ \to \mathbb{R}^{n\times 1}$ is the state vector; $\boldsymbol{u}_c(t)$:$\mathbb{R}^+ \to \mathbb{R}^{m_c\times 1}$ and $\boldsymbol{u}_{dk}$:$\mathbb{N} \to \mathbb{R}^{m_d\times 1}$ are the control inputs; and assuming equal input/output dimensions, $\boldsymbol{y}_c(t)$:$\mathbb{R}^+ \to \mathbb{R}^{m_c\times 1}$ and $\boldsymbol{y}_{dk}$:$\mathbb{N} \to \mathbb{R}^{m_d\times 1}$ are the output vectors. The continuous-time state-space matrices $\boldsymbol{A}_c(t)$, $\boldsymbol{B}_c(t)$, $\boldsymbol{C}_c(t)$, and $\boldsymbol{D}_c(t)$, as well as the discrete-time $\boldsymbol{A}_{dk}$, $\boldsymbol{B}_{dk}$, $\boldsymbol{C}_{dk}$, and $\boldsymbol{D}_{dk}$, are all dimensioned appropriately. A hybrid LTI system can be represented in an almost identical manner, but with constant continuous-time $\boldsymbol{A}_c$, $\boldsymbol{B}_c$, $\boldsymbol{C}_c$, and $\boldsymbol{D}_c$, as well as constant discrete-time $\boldsymbol{A}_d$, $\boldsymbol{B}_d$, $\boldsymbol{C}_d$, and $\boldsymbol{D}_d$ matrices. Section II.A builds the foundations of hybrid passivity using some definitions and lemmas, and it extends the celebrated passivity theorem to hybrid systems. Section II.B then follows by providing a set of conditions that could be used for passivity-based design of hybrid systems.

A. Definitions, Lemmas, and Hybrid Passivity Theorem

Definitions 2.1 and 2.2 extend the finite 2-norm spaces to hybrid systems (from [1] Chap. 2, for example), and Definition 2.3 provides a hybrid extension of the inner product and norm operations.

Definition 2.1: The hybrid $\mathcal{L}_2^h$ space is defined as the Cartesian product of the continuous- and discrete-time finite norm spaces ($\mathcal{L}_2^h \triangleq \mathcal{L}_2 \times l_2$), such that a hybrid vector function $\boldsymbol{v} = \{\boldsymbol{v}_c(t), \boldsymbol{v}_{dk}\} \in \mathcal{L}_2^h$ if both $\boldsymbol{v}_c(t) \in \mathcal{L}_2$ and $\boldsymbol{v}_{dk} \in l_2$. More precisely,

$$\mathcal{L}_2^h \triangleq \left\{ \boldsymbol{v} = \{\boldsymbol{v}_c(t), \boldsymbol{v}_{dk}\} \,\middle|\, \int_0^\infty \boldsymbol{v}_c^{\mathrm{T}}(t)\boldsymbol{v}_c(t)\,\mathrm{d}t < \infty, \sum_{k=1}^{\infty} \boldsymbol{v}_{dk}^{\mathrm{T}}\boldsymbol{v}_{dk} < \infty \right\}$$

Definition 2.2: The hybrid extended $\mathcal{L}_{2e}^h$ space is defined as the Cartesian product of the extended continuous- and discrete-time finite norm spaces ($\mathcal{L}_{2e}^h \triangleq \mathcal{L}_{2e} \times l_{2e}$), such that a truncated hybrid vector function (that becomes identically zero after some time $t = \hat{t}$ between impulses $t_{\hat{N}-1} < \hat{t} < t_{\hat{N}}$) $\boldsymbol{v}_{\hat{t}} = \{\boldsymbol{v}_{c\hat{t}}(t), \boldsymbol{v}_{dk\hat{t}}\} \in \mathcal{L}_{2e}^h$ if both $\boldsymbol{v}_{c\hat{t}}(t) \in \mathcal{L}_{2e}$ and $\boldsymbol{v}_{dk\hat{t}} \in l_{2e}$. More precisely,

$$\mathcal{L}_{2e}^h \triangleq \left\{ \boldsymbol{v} = \{\boldsymbol{v}_c(t), \boldsymbol{v}_{dk}\} \,\middle|\, \int_0^{\hat{t}} \boldsymbol{v}_c^{\mathrm{T}}(t)\boldsymbol{v}_c(t)\,\mathrm{d}t < \infty, \sum_{k=1}^{\hat{N}-1} \boldsymbol{v}_{dk}^{\mathrm{T}}\boldsymbol{v}_{dk} < \infty, 0 < \hat{t} < \infty, t_{\hat{N}-1} < \hat{t} < t_{\hat{N}} \right\}$$

where $\hat{t}$ denotes the truncation time ($0 < \hat{t} < \infty$) and, after $\hat{N} - 1$ impulses, $t_{\hat{N}-1} < \hat{t} < t_{\hat{N}}$. The variable $\hat{t}$ is considered to be strictly less than $t_{\hat{N}}$ in order to avoid ambiguity about whether or not there is a nonzero impulsive thrust at time $t_{\hat{N}}$. Consistent with the definition of $\hat{N} - 1$ being the last nonzero thrust, the impulsive thrust at $t_{\hat{N}}$ is set to zero.

Definition 2.3: The hybrid (truncated) inner product of two hybrid vector functions, $\boldsymbol{v} \in \mathcal{L}_2^h$ and $\boldsymbol{w} \in \mathcal{L}_2^h$ (or $\boldsymbol{v} \in \mathcal{L}_{2e}^h$ and $\boldsymbol{w} \in \mathcal{L}_{2e}^h$), is defined as Follows:

$$\langle \boldsymbol{v}|\boldsymbol{w}\rangle^h \triangleq \int_0^\infty \boldsymbol{v}_c^{\mathrm{T}}(t)\boldsymbol{w}_c(t)\,\mathrm{d}t + \sum_{k=1}^{\infty} \boldsymbol{v}_{dk}^{\mathrm{T}}\boldsymbol{w}_{dk}$$

$$\langle \boldsymbol{v}|\boldsymbol{w}\rangle_{\hat{t}}^h \triangleq \int_0^{\hat{t}} \boldsymbol{v}_c^{\mathrm{T}}(t)\boldsymbol{w}_c(t)\,\mathrm{d}t + \sum_{k=1}^{\hat{N}-1} \boldsymbol{v}_{dk}^{\mathrm{T}}\boldsymbol{w}_{dk}$$

For a vector $\boldsymbol{v} \in \mathcal{L}_2^h$ or $\boldsymbol{v} \in \mathcal{L}_{2e}^h$, the hybrid norm or hybrid truncated norm is defined as $\|\boldsymbol{v}\|_2^h \triangleq (\langle \boldsymbol{v}|\boldsymbol{v}\rangle^h)^{1/2}$ or $\|\boldsymbol{v}\|_{2\hat{t}}^h \triangleq (\langle \boldsymbol{v}|\boldsymbol{v}\rangle_{\hat{t}}^h)^{1/2}$, respectively.

Similar to the classical inner product and $\mathcal{L}_2$ or l_2 norms, the hybrid (truncated) inner products and norms defined in Definition 2.3 satisfy the Cauchy–Schwarz inequality, as stated in Lemma 2.1 as follows:

Lemma 2.1: For two hybrid vector functions $\boldsymbol{v} \in \mathcal{L}_2^h$ and $\boldsymbol{w} \in \mathcal{L}_2^h$, or $\boldsymbol{v} \in \mathcal{L}_{2e}^h$ and $\boldsymbol{w} \in \mathcal{L}_{2e}^h$, the Cauchy–Schwarz inequality holds using hybrid (truncated) inner products and norms:

$$\langle \boldsymbol{v}|\boldsymbol{w}\rangle^h \leqslant \|\boldsymbol{v}\|_2^h \cdot \|\boldsymbol{w}\|_2^h \tag{3a}$$

$$\langle \boldsymbol{v}|\boldsymbol{w}\rangle_{\hat{t}}^h \leqslant \|\boldsymbol{v}\|_{2\hat{t}}^h \cdot \|\boldsymbol{w}\|_{2\hat{t}}^h \tag{3b}$$

Proof: Refer to the Appendix of this paper.

With the preliminary definitions in place, the notion of "hybrid (input strict) passivity" [an extension of classical passivity as defined in ([37] Chap. 2), for example] is presented in Definition 2.4 below. Theorem 2.1 provides conditions pertinent to hybrid systems under which (input strict) passivity is guaranteed. These conditions parallel those applicable to classical passivity, provided in ([37] Chap. 2) and ([38] definition 1), for instance.

Definition 2.4: A hybrid system $\boldsymbol{y} = \mathcal{G}^h\boldsymbol{u}$, modeled by Eqs. (1) and (2), is passive if

$$\langle \boldsymbol{y}|\boldsymbol{u}\rangle_{\hat{t}}^h \geqslant \beta, \quad \forall\, \boldsymbol{u} \in \mathcal{L}_{2e}^h, \quad \forall\, \hat{t} \in \mathbb{R}^+ \tag{4}$$

for some real constant $\beta \leqslant 0$ that relates to the initial energy of the system. If the initial conditions are zero, $\beta = 0$. Similarly, it is input strictly passive if there exists $\epsilon > 0$ such that

$$\langle \boldsymbol{y}|\boldsymbol{u}\rangle_{\hat{t}}^h \geqslant \beta + \epsilon(\|\boldsymbol{u}\|_{2\hat{t}}^h)^2, \quad \forall\, \boldsymbol{u} \in \mathcal{L}_{2e}^h, \quad \forall\, \hat{t} \in \mathbb{R}^+ \tag{5}$$

for some real constant $\beta \leqslant 0$.

Theorem 2.1: A hybrid system $\boldsymbol{y} = \mathcal{G}^h\boldsymbol{u}$, represented by Eqs. (1) and (2), is passive if there exists a piecewise continuous scalar function, termed a "hybrid storage function," $V(\boldsymbol{x}(t)) \geqslant 0$, such that the following conditions hold within each time interval: $t \in (t_\kappa, t_{\kappa+1})$, $\kappa \in \mathbb{W}$. Or, at each impulse time, $t = t_k$, $k \in \mathbb{N}$:

$$V(t_b) - V(t_a) \leqslant \int_{t_a}^{t_b} \boldsymbol{y}_c^{\mathrm{T}}(\tau)\boldsymbol{u}_c(\tau)\,\mathrm{d}\tau, \qquad t_\kappa < t_a \leqslant t_b < t_{\kappa+1} \tag{6a}$$

$$V(t_k^+) - V(t_k^-) \leqslant \boldsymbol{y}_{dk}^{\mathrm{T}}\boldsymbol{u}_{dk} \tag{6b}$$

where $t_0^+ = 0$, and the state dependence of V is omitted for brevity. Furthermore, the system is input strictly passive if there also exist constants $\epsilon_{c\kappa} > 0$, $\kappa \in \mathbb{W}$, and $\epsilon_{dk} > 0$, $k \in \mathbb{N}$, such that

$$V(t_b) - V(t_a) \leqslant \int_{t_a}^{t_b} \boldsymbol{y}_c^{\mathrm{T}}(\tau)\boldsymbol{u}_c(\tau)\,\mathrm{d}\tau - \epsilon_{c\kappa}\int_{t_a}^{t_b} \boldsymbol{u}_c^{\mathrm{T}}(\tau)\boldsymbol{u}_c(\tau)\,\mathrm{d}\tau, \quad t_\kappa < t_a \leqslant t_b < t_{\kappa+1} \tag{7a}$$

$$V(t_k^+) - V(t_k^-) \leqslant \boldsymbol{y}_{dk}^{\mathrm{T}}\boldsymbol{u}_{dk} - \epsilon_{dk}\boldsymbol{u}_{dk}^{\mathrm{T}}\boldsymbol{u}_{dk} \tag{7b}$$

Proof: Refer to the Appendix of this paper.

Thus far, only (input strict) passivity of a single plant has been considered. Presented in Theorem 2.2 is a "hybrid passivity theorem" [a general case of which was considered in ([11] theorem 1)] that can act as a useful tool to design a feedback controller for the hybrid system of interest in this document. Once again, this is a hybrid extension of the well-known passivity theorem, stated and proved in ([1] Chap. VI), among other sources.

Theorem 2.2: Consider the negative feedback interconnection, illustrated in Fig. 1, of a hybrid plant $\boldsymbol{y} = \mathscr{G}^h\boldsymbol{u}$ with a hybrid controller $\hat{\boldsymbol{y}} = \mathscr{H}^h\hat{\boldsymbol{u}}$, with disturbances such that $\boldsymbol{u} = \boldsymbol{d} - \hat{\boldsymbol{y}}$. If $\mathscr{G}^h$ is passive and $\mathscr{H}^h$ is input strictly passive, then $\boldsymbol{d} \in \mathcal{L}_2^h$ implies $\boldsymbol{y} \in \mathcal{L}_2^h$ as well.

Proof: From passivity of $\mathscr{G}^h$ by Definition 2.4,

$$\langle \boldsymbol{y}|\boldsymbol{u}\rangle_{\hat{t}}^h \geqslant \beta_1, \quad \langle \boldsymbol{y}|\boldsymbol{d}-\hat{\boldsymbol{y}}\rangle_{\hat{t}}^h = \langle \boldsymbol{y}|\boldsymbol{d}\rangle_{\hat{t}}^h - \langle \boldsymbol{y}|\hat{\boldsymbol{y}}\rangle_{\hat{t}}^h \geqslant \beta_1, \quad \forall\ \boldsymbol{u} \in \mathcal{L}_{2e}^h,\ \hat{t} > 0 \tag{8}$$

for some real constant $\beta_1 \leqslant 0$, where linearity of the inner product operation is used. Similarly, from input strict passivity of $\mathscr{H}^h$ by Definition 2.4.

$$\exists \epsilon > 0, \qquad \langle \hat{\boldsymbol{y}}|\boldsymbol{y}\rangle_{\hat{t}}^h = \langle \boldsymbol{y}|\hat{\boldsymbol{y}}\rangle_{\hat{t}}^h \geqslant \beta_2 + \epsilon(\|\hat{\boldsymbol{y}}\|_{2\hat{t}}^h)^2, \quad \forall\ \boldsymbol{y} \in \mathcal{L}_{2e}^h, \qquad \hat{t} > 0 \tag{9}$$

for some real constant $\beta_2 \leqslant 0$, where commutativity of the inner product operation is used. Rearranging Eq. (8) and using Eq. (9) results in the following:

$$\beta_1 + \beta_2 + \epsilon(\|\boldsymbol{y}\|_{2\hat{t}}^h)^2 \leqslant \langle \boldsymbol{y}|\boldsymbol{d}\rangle_{\hat{t}}^h \leqslant \|\boldsymbol{y}\|_{2\hat{t}}^h \cdot \|\boldsymbol{d}\|_{2\hat{t}}^h \tag{10}$$

where the Cauchy–Schwarz inequality of Lemma 2.1 is used. Finally, dividing Eq. (10) by $\epsilon\|\boldsymbol{y}\|_{2\hat{t}}^h$ and letting $\hat{t} \to \infty$ yields the following:

$$\|\boldsymbol{y}\|_2^h \leqslant \frac{1}{\epsilon}\|\boldsymbol{d}\|_2^h - \frac{\beta_1 + \beta_2}{\epsilon\|\boldsymbol{y}\|_2^h} \tag{11}$$

for some real constants $\beta_1 \leqslant 0$ and $\beta_2 \leqslant 0$, which implies that, if $\|\boldsymbol{d}\|_2^h < \infty$ (i.e., $\boldsymbol{d} \in \mathcal{L}_2^h$), then so is $\|\boldsymbol{y}\|_2^h < \infty$ (i.e., $\boldsymbol{y} \in \mathcal{L}_2^h$), as required. This conclusion follows from assuming, by way of contradiction, that $\|\boldsymbol{y}\|_2^h \to \infty$ as $t \to \infty$, and observing that the right-hand side of Eq. (11) approaches $\|\boldsymbol{d}\|_2^h/\epsilon < \infty$. This places a finite upper bound on $\|\boldsymbol{y}\|_2^h$ that conflicts with the original assumption, hence proving that, indeed, $\|\boldsymbol{y}\|_2^h < \infty$.

Theorem 2.2 suggests a useful passivity-based design approach that involves specifying the plant's continuous- and discrete-time outputs such that it becomes passive, and then feeding the outputs back via an input strictly passive controller, hence ensuring the stability of the overall feedback system. An input strictly passive controller can be as simple as the proportional controller described later in Sec. IV.C

$$\hat{\boldsymbol{y}} = \{\hat{\boldsymbol{y}}_c(t), \hat{\boldsymbol{y}}_{dk}\} = \{k_c\boldsymbol{y}_c(t), k_d\boldsymbol{y}_{dk}\}$$

with $k_c > 0$ and $k_d > 0$; or, it can have a more sophisticated design, such as that of the dynamic compensator detailed later in Sec. IV.D. Section II.B presents some conditions that could be used in designing a passive plant with a time-varying model, whereas Sec. II.C lists the algebraic analog of these conditions, to be used for an input strictly passive controller with time-invariant state-space matrices.

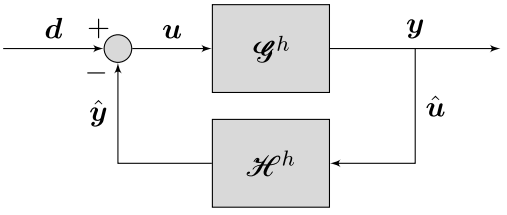

Fig. 1 Negative feedback interconnection of a hybrid plant and a hybrid controller.

B. Hybrid Extended KYP Conditions

The classical KYP conditions focus on LTI systems. They establish an equivalence between a set of equations involving the state-space model's matrices and the existence of some positive-definite matrices that also manifest themselves in the equations. A generalization of the KYP conditions for passivity of impulsive (dynamical) systems is presented in ([10] corollary 5), and an extension of the continuous portion to time-varying systems is provided in ([16] theorem 3.1). These results, together with the discrete-time equivalent of the KYP conditions presented in [39], can all be combined to provide a set of hybrid extended KYP conditions, presented in Theorem 2.3 in the following, that could be used for the LTV hybrid system studied in this paper.

Theorem 2.3: Consider the hybrid system $\boldsymbol{y} = \mathscr{G}^h\boldsymbol{u}$ represented by Eqs. (1) and (2). If there exists a symmetric positive-semidefinite matrix $\boldsymbol{P}(t)$:$\mathbb{R}^+ \to \mathbb{R}^{n\times n}$, real continuous-time matrices $\boldsymbol{L}_c(t)$:$\mathbb{R}^+ \to \mathbb{R}^{m_c\times n}$ and $\boldsymbol{W}_c(t)$:$\mathbb{R}^+ \to \mathbb{R}^{m_c\times m_c}$, and real discrete-time matrices $\boldsymbol{L}_{dk}$:$\mathbb{N} \to \mathbb{R}^{m_d\times n}$ and $\boldsymbol{W}_{dk}$:$\mathbb{N} \to \mathbb{R}^{m_d\times m_d}$, such that the following conditions hold for some $\epsilon_{c\kappa} \geqslant 0$, $\kappa \in \mathbb{W}$, and $\epsilon_{dk} \geqslant 0$, $k \in \mathbb{N}$

$$\boldsymbol{0} = \dot{\boldsymbol{P}}(t) + \boldsymbol{A}_c^\intercal(t)\boldsymbol{P}(t) + \boldsymbol{P}(t)\boldsymbol{A}_c(t) + \boldsymbol{L}_c^\intercal(t)\boldsymbol{L}_c(t) \tag{12a}$$

$$\boldsymbol{0} = \boldsymbol{P}(t)\boldsymbol{B}_c(t) - \boldsymbol{C}_c^\intercal(t) + \boldsymbol{L}_c^\intercal(t)\boldsymbol{W}_c(t) \tag{12b}$$

$$\boldsymbol{0} = -2\epsilon_{c\kappa}1 + \boldsymbol{D}_c(t) + \boldsymbol{D}_c^\intercal(t) - \boldsymbol{W}_c^\intercal(t)\boldsymbol{W}_c(t) \tag{12c}$$

$$\boldsymbol{0} = \boldsymbol{A}_{dk}^\intercal\boldsymbol{P}(t_k^+)\boldsymbol{A}_{dk} - \boldsymbol{P}(t_k^-) + \boldsymbol{L}_{dk}^\intercal\boldsymbol{L}_{dk} \tag{12d}$$

$$\boldsymbol{0} = \boldsymbol{A}_{dk}^\intercal\boldsymbol{P}(t_k^+)\boldsymbol{B}_{dk} - \boldsymbol{C}_{dk}^\intercal + \boldsymbol{L}_{dk}^\intercal\boldsymbol{W}_{dk} \tag{12e}$$

$$\boldsymbol{0} = -2\epsilon_{dk}1 + \boldsymbol{D}_{dk} + \boldsymbol{D}_{dk}^\intercal - \boldsymbol{B}_{dk}^\intercal\boldsymbol{P}(t_k^+)\boldsymbol{B}_{dk} - \boldsymbol{W}_{dk}^\intercal\boldsymbol{W}_{dk} \tag{12f}$$

then the LTV system $\mathscr{G}^h$ is passive if all $\epsilon_{c\kappa} = \epsilon_{dk} \equiv 0$, and it is input strictly passive if all $\epsilon_{c\kappa} > 0$ and $\epsilon_{dk} > 0$.

Proof: A similar approach to that in [16] (for the continuous portion) is followed using a quadratic storage function:

$$V(\boldsymbol{x}(t)) = \frac{1}{2}\boldsymbol{x}^\intercal(t)\boldsymbol{P}(t)\boldsymbol{x}(t) \tag{13}$$

the time derivative of which can be written, using Eq. (1a) and rearranging, as follows:

$$\dot{V} = \frac{1}{2}\boldsymbol{x}^\intercal(\dot{\boldsymbol{P}} + \boldsymbol{A}_c^\intercal\boldsymbol{P} + \boldsymbol{P}\boldsymbol{A}_c)\boldsymbol{x} + \boldsymbol{x}^\intercal\boldsymbol{P}\boldsymbol{B}_c\boldsymbol{u}_c \tag{14}$$

where the time dependence of all variables is omitted for clarity. Rearranging the conditions in Eqs. (12a) and (12b) and substituting the results in Eq. (14) yields the following:

$$\dot{V} = -\frac{1}{2}(\boldsymbol{L}_c\boldsymbol{x})^\intercal\boldsymbol{L}_c\boldsymbol{x} + (\boldsymbol{C}_c\boldsymbol{x})^\intercal\boldsymbol{u}_c - (\boldsymbol{L}_c\boldsymbol{x})^\intercal\boldsymbol{W}_c\boldsymbol{u}_c \tag{15}$$

in which Eq. (1b) for the output of the continuous model can be used to obtain, upon rearranging,

$$\dot{V} = \boldsymbol{y}_c^\intercal\boldsymbol{u}_c - \frac{1}{2}[(\boldsymbol{L}_c\boldsymbol{x})^\intercal\boldsymbol{L}_c\boldsymbol{x} + 2(\boldsymbol{L}_c\boldsymbol{x})^\intercal\boldsymbol{W}_c\boldsymbol{u}_c + 2\boldsymbol{u}_c^\intercal\boldsymbol{D}_c\boldsymbol{u}_c] \tag{16}$$

Further rearranging Eq. (16) and noting that

$$\boldsymbol{u}_c^\intercal\boldsymbol{D}_c\boldsymbol{u}_c = (\boldsymbol{D}_c\boldsymbol{u}_c)^\intercal\boldsymbol{u}_c = \boldsymbol{u}_c^\intercal\boldsymbol{D}_c^\intercal\boldsymbol{u}_c$$

we have the following:

$$\begin{aligned}\boldsymbol{y}_c^{\intercal}\boldsymbol{u}_c &= \dot{V} + \frac{1}{2}[(\boldsymbol{L}_c\boldsymbol{x})^{\intercal}\boldsymbol{L}_c\boldsymbol{x} + 2(\boldsymbol{L}_c\boldsymbol{x})^{\intercal}\boldsymbol{W}_c\boldsymbol{u}_c + (\boldsymbol{W}_c\boldsymbol{u}_c)^{\intercal}\boldsymbol{W}_c\boldsymbol{u}_c \\ &\quad + 2\epsilon_{c\kappa}\boldsymbol{u}_c^{\intercal}\boldsymbol{u}_c] \\ &= \dot{V} + \frac{1}{2}(\boldsymbol{L}_c\boldsymbol{x} + \boldsymbol{W}_c\boldsymbol{u}_c)^{\intercal}(\boldsymbol{L}_c\boldsymbol{x} + \boldsymbol{W}_c\boldsymbol{u}_c) + \epsilon_{c\kappa}\boldsymbol{u}_c^{\intercal}\boldsymbol{u}_c \end{aligned} \tag{17}$$

where the condition in Eq. (12c) is evoked. Equation (17) can be integrated from time t_a to t_b within any time interval $t_\kappa < t_a \leqslant t_b < t_{\kappa+1}$:

$$\begin{aligned}\int_{t_a}^{t_b} \boldsymbol{y}_c^{\intercal}\boldsymbol{u}_c \,\mathrm{d}\tau &= V(t_b) - V(t_a) + \frac{1}{2}\int_{t_a}^{t_b} |\boldsymbol{L}_c\boldsymbol{x} + \boldsymbol{W}_c\boldsymbol{u}_c|^2 \,\mathrm{d}t \\ &\quad + \epsilon_{c\kappa}\int_{t_a}^{t_b} \boldsymbol{u}_c^{\intercal}\boldsymbol{u}_c \,\mathrm{d}\tau \end{aligned} \tag{18}$$

but the integral of a norm is always nonnegative; thus,

$$\int_{t_a}^{t_b} \boldsymbol{y}_c^{\intercal}(\tau)\boldsymbol{u}_c(\tau)\,\mathrm{d}\tau - \epsilon_{c\kappa}\int_{t_a}^{t_b} \boldsymbol{u}_c^{\intercal}(\tau)\boldsymbol{u}_c(\tau)\,\mathrm{d}\tau \geqslant V(t_b) - V(t_a) \tag{19}$$

as required by Eq. (7a) for some $\epsilon_{c\kappa} > 0$. If $\epsilon_{c\kappa} \equiv 0$, then Eq. (19) reduces to the following:

$$\int_{t_a}^{t_b} \boldsymbol{y}_c^{\intercal}(\tau)\boldsymbol{u}_c(\tau)\,\mathrm{d}\tau \geqslant V(t_b) - V(t_a) \tag{20}$$

as required by Eq. (6a).

Using the same storage function for the discrete dynamics, the change in the function's value over an impulse can be found by taking the difference between Eq. (13) computed after and before an impulse time t_k, using Eq. (2a) for the discrete-time state dynamics. We have

$$\begin{aligned}V(t_k^+) - V(t_k^-) &= \frac{1}{2}(\boldsymbol{A}_d\boldsymbol{x}_k^- + \boldsymbol{B}_d\boldsymbol{u}_k)^{\intercal}\boldsymbol{P}_k^+(\boldsymbol{A}_d\boldsymbol{x}_k^- + \boldsymbol{B}_d\boldsymbol{u}_k) - \frac{1}{2}\boldsymbol{x}_k^{-\intercal}\boldsymbol{P}_k^-\boldsymbol{x}_k^- \\ &= \frac{1}{2}\boldsymbol{x}_k^{-\intercal}(\boldsymbol{A}_d^{\intercal}\boldsymbol{P}_k^+\boldsymbol{A}_d - \boldsymbol{P}_k^-)\boldsymbol{x}_k^- + \boldsymbol{u}_d^{\intercal}\boldsymbol{B}_d^{\intercal}\boldsymbol{P}_k^+\boldsymbol{A}_d\boldsymbol{x}_k^- \\ &\quad + \frac{1}{2}\boldsymbol{u}_d^{\intercal}\boldsymbol{B}_d^{\intercal}\boldsymbol{P}_k^+\boldsymbol{B}_d\boldsymbol{u}_d \end{aligned} \tag{21}$$

where $\boldsymbol{x}_k^{\pm} \triangleq \boldsymbol{x}(t_k^{\pm})$ and $\boldsymbol{P}_k^{\pm} \triangleq \boldsymbol{P}(t_k^{\pm})$, and index dependence of all other variables is omitted for clarity. Substituting the conditions in Eqs. (12d) and (12e) of the theorem into Eq. (21) yields the following:

$$\begin{aligned}\Delta V_k &= \frac{1}{2}\boldsymbol{x}_k^{-\intercal}(\cancel{\boldsymbol{P}_k^-} - \boldsymbol{L}_d^{\intercal}\boldsymbol{L}_d - \cancel{\boldsymbol{P}_k^-})\boldsymbol{x}_k^- + \boldsymbol{u}_d^{\intercal}(\boldsymbol{C}_d - \boldsymbol{W}_d^{\intercal}\boldsymbol{L}_d)\boldsymbol{x}_k^- \\ &\quad + \frac{1}{2}\boldsymbol{u}_d^{\intercal}(\boldsymbol{D}_d + \boldsymbol{D}_d^{\intercal} - \boldsymbol{W}_d^{\intercal}\boldsymbol{W}_d - 2\epsilon_{dk}1)\boldsymbol{u}_d \\ &= \boldsymbol{u}_d^{\intercal}(\boldsymbol{C}_d\boldsymbol{x}_k^- + \boldsymbol{D}_d\boldsymbol{u}_d) - \frac{1}{2}[(\boldsymbol{L}_d\boldsymbol{x}_k^-)^{\intercal}\boldsymbol{L}_d\boldsymbol{x}_k^- + 2(\boldsymbol{L}_d\boldsymbol{x}_k^-)^{\intercal}\boldsymbol{W}_d\boldsymbol{u}_d \\ &\quad + (\boldsymbol{W}_d\boldsymbol{u}_d)^{\intercal}\boldsymbol{W}_d\boldsymbol{u}_d] - \epsilon_{dk}\boldsymbol{u}_d^{\intercal}\boldsymbol{u}_d \end{aligned} \tag{22}$$

where, similar to the continuous portion,

$$\boldsymbol{u}_d^{\intercal}\boldsymbol{D}_d\boldsymbol{u}_d = (\boldsymbol{D}_d\boldsymbol{u}_d)^{\intercal}\boldsymbol{u}_d = \boldsymbol{u}_d^{\intercal}\boldsymbol{D}_d^{\intercal}\boldsymbol{u}_d$$

is used. Finally, using Eq. (2b) for the output of the discrete model and recognizing the second set of terms in Eq. (22) as an inner product, upon rearranging the result, we obtain the following:

$$\boldsymbol{y}_d^{\intercal}\boldsymbol{u}_d = V(t_k^+) - V(t_k^-) + \frac{1}{2}|\boldsymbol{L}_d\boldsymbol{x}_k^- + \boldsymbol{W}_d\boldsymbol{u}_d|^2 + \epsilon_{dk}\boldsymbol{u}_d^{\intercal}\boldsymbol{u}_d \tag{23}$$

But, a vector norm is always nonnegative; thus,

$$\boldsymbol{y}_{dk}^{\intercal}\boldsymbol{u}_{dk} - \epsilon_{dk}\boldsymbol{u}_d^{\intercal}\boldsymbol{u}_d \geqslant V(t_k^+) - V(t_k^-) \tag{24}$$

as required by Eq. (7b) for some $\epsilon_{dk} > 0$. If $\epsilon_{dk} \equiv 0$, then Eq. (24) reduces to the following:

$$\boldsymbol{y}_{dk}^{\intercal}\boldsymbol{u}_{dk} \geqslant V(t_k^+) - V(t_k^-) \tag{25}$$

as required by Eq. (6b).

Together with Eq. (20), Eq. (25) proves the hybrid passivity of the system; and together with Eq. (19), Eq. (24) establishes the hybrid input strict passivity of the system, as defined in Definition (2.4) and according to Theorem (2.2). □

Noting the resemblance of Eq. (12a) to the well-known Lyapunov equation, $\boldsymbol{P}(t)$ will hereafter be referred to as the "Lyapunov solution." In addition, the set of conditions in Eq. (12) will be called the "hybrid extended KYP conditions" and will be used in Sec. IV.B for passivity-based design of the plant output dynamics.

C. Hybrid Algebraic KYP Conditions

Theorem 2.4 specializes the hybrid KYP conditions of Theorem 2.3 to a hybrid LTI system, in which the state-space matrices are constant, for which the differential and difference equations reduce to algebraic equations, and for which the Lyapunov solution $\boldsymbol{P}$ remains constant over time and at each impulse. These conditions follow directly from the results of [10] (although input strict passivity is not treated explicitly in that paper), but they can also be considered as special (time-invariant) analog of the hybrid extended KYP conditions presented in Sec. II.B.

Theorem 2.4: Consider the hybrid system $\boldsymbol{y} = \mathscr{G}^h\boldsymbol{u}$ represented by Eqs. (1) and (2). If there exists a symmetric positive-semidefinite matrix $\bar{P} \in \mathbb{R}^{n\times n}$, real continuous-time matrices $\boldsymbol{L}_c \in \mathbb{R}^{m_c\times n}$ and $\boldsymbol{W}_c \in \mathbb{R}^{m_c\times m_c}$, and real discrete-time matrices $\boldsymbol{L}_d \in \mathbb{R}^{m_d\times n}$ and $\boldsymbol{W}_d \in \mathbb{R}^{m_d\times m_d}$, such that the following conditions hold for some $\epsilon_{c\kappa} \geqslant 0$, $\kappa \in \mathbb{W}$, and $\epsilon_{dk} \geqslant 0$, $k \in \mathbb{N}$:

$$\boldsymbol{0} = \boldsymbol{A}_c^{\intercal}\bar{\boldsymbol{P}} + \bar{\boldsymbol{P}}\boldsymbol{A}_c + \boldsymbol{L}_c^{\intercal}\boldsymbol{L}_c \tag{26a}$$

$$\boldsymbol{0} = \bar{\boldsymbol{P}}\boldsymbol{B}_c - \boldsymbol{C}_c^{\intercal} + \boldsymbol{L}_c^{\intercal}\boldsymbol{W}_c \tag{26b}$$

$$\boldsymbol{0} = -2\epsilon_c\boldsymbol{1} + \boldsymbol{D}_c + \boldsymbol{D}_c^{\intercal} - \boldsymbol{W}_c^{\intercal}\boldsymbol{W}_c \tag{26c}$$

$$\boldsymbol{0} = \boldsymbol{A}_d^{\intercal}\bar{\boldsymbol{P}}\boldsymbol{A}_d - \bar{\boldsymbol{P}} + \boldsymbol{L}_d^{\intercal}\boldsymbol{L}_d \tag{26d}$$

$$\boldsymbol{0} = \boldsymbol{A}_d^{\intercal}\bar{\boldsymbol{P}}\boldsymbol{B}_d - \boldsymbol{C}_d^{\intercal} + \boldsymbol{L}_d^{\intercal}\boldsymbol{W}_d \tag{26e}$$

$$\boldsymbol{0} = -2\epsilon_d\boldsymbol{1} + \boldsymbol{D}_d + \boldsymbol{D}_d^{\intercal} - \boldsymbol{B}_d^{\intercal}\bar{\boldsymbol{P}}\boldsymbol{B}_d - \boldsymbol{W}_d^{\intercal}\boldsymbol{W}_d \tag{26f}$$

then the LTI system $\mathscr{G}^h$ is passive if $\epsilon_c = \epsilon_d \equiv 0$, and it is input strictly passive if all $\epsilon_c > 0$ and $\epsilon_d > 0$.

Proof: Refer to the proof of theorem 14 of [10], of which this theorem is a corollary, with the general quadratic supply rates

$$r_c = \boldsymbol{y}_c^{\intercal}\boldsymbol{\mathcal{Q}}_c\boldsymbol{y}_c + 2\boldsymbol{y}_c^{\intercal}\boldsymbol{\mathcal{S}}_c\boldsymbol{u}_c + \boldsymbol{u}_c^{\intercal}\boldsymbol{\mathcal{R}}_c\boldsymbol{u}_c$$

and

$$r_d = \boldsymbol{y}_d^{\intercal}\boldsymbol{\mathcal{Q}}_d\boldsymbol{y}_d + 2\boldsymbol{y}_d^{\intercal}\boldsymbol{\mathcal{S}}_d\boldsymbol{u}_d + \boldsymbol{u}_d^{\intercal}\boldsymbol{\mathcal{R}}_d\boldsymbol{u}_d$$

Are set using the specific parameters $\boldsymbol{\mathcal{Q}}_c = \boldsymbol{0}, \boldsymbol{\mathcal{S}}_c = \boldsymbol{1}, \boldsymbol{\mathcal{R}}_c = -2\epsilon_c\boldsymbol{1}$, $\boldsymbol{\mathcal{Q}}_d = \boldsymbol{0}, \boldsymbol{\mathcal{S}}_d = \boldsymbol{1}$, and $\boldsymbol{\mathcal{R}}_d = -2\epsilon_d\boldsymbol{1}$, where $\epsilon_c = \epsilon_d \equiv 0$ for passivity, and $\epsilon_c > 0$ and $\epsilon_d > 0$ for input strict passivity. □

Noting the resemblance of Eq. (26a) to the well-known Lyapunov equation, $\bar{\boldsymbol{P}}$ will hereafter be referred to as the "algebraic Lyapunov solution." In addition, the set of conditions in Eq. (26) will be called the "hybrid algebraic KYP conditions" and will be used in Sec. IV.D to design an input strictly passive controller.

III. Spacecraft Kinematics and Dynamics

The passivity-based hybrid control strategy using the associated KYP conditions considered thus far is applied to the problem of attitude control via magnetic actuators augmented with auxiliary impulsive thrusters. A Keplerian orbit is assumed and used to determine the spacecraft's position vector $\boldsymbol{r}_G(t)$ at any given time. Using this information, the tilted dipole model of Earth's magnetic field (described in appendix H of [19]) can be used to estimate the magnetic field vector $\boldsymbol{b}_G(t)$. The body-fixed frame representations of these vectors are then obtained using $\boldsymbol{b}_B = \boldsymbol{C}_{BG}\boldsymbol{b}_G$ and $\boldsymbol{r}_B = \boldsymbol{C}_{BG}\boldsymbol{r}_G$, where $\boldsymbol{C}_{BG}$ denotes the rotation matrix from the inertial frame to the body-fixed frame. Adopting the four-parameter set of quaternions, $\boldsymbol{\epsilon} = [\,\epsilon_1 \quad \epsilon_2 \quad \epsilon_3\,]^\intercal$ and η; to represent the spacecraft's attitude, the rotation matrix can be computed using $\boldsymbol{C}_{BG} = (\eta^2 - \boldsymbol{\epsilon}^\intercal\boldsymbol{\epsilon})1_{3\times3} + 2\boldsymbol{\epsilon}\boldsymbol{\epsilon}^\intercal - 2\eta\boldsymbol{\epsilon}^\times$ ([40] Chap. 2).

Assuming a total of $N-1$ impulsive thrusts applied within the control interval, the rotational kinematics and dynamics can be described as follows ([40] Chaps. 2 and 4):

$$\begin{bmatrix}\dot{\boldsymbol{\epsilon}}\\ \dot{\eta}\end{bmatrix} = \frac{1}{2}\begin{bmatrix}\eta 1_{3\times3} + \boldsymbol{\epsilon}^\times\\ -\boldsymbol{\epsilon}^\intercal\end{bmatrix}\boldsymbol{\omega} \tag{27a}$$

$$\boldsymbol{I}\dot{\boldsymbol{\omega}} + \boldsymbol{\omega}^\times\boldsymbol{I}\boldsymbol{\omega} = \boldsymbol{m}^\times\boldsymbol{b}_B + \sum_{k=1}^{N-1}\boldsymbol{n}_k\delta(t-t_k) + \boldsymbol{\tau}_{\text{dist}} \tag{27b}$$

Where the first and second terms on the right-hand side of Eq. (27b) represent the magnetic torquers' and thrusters' contributions to the control torques, respectively, with the Dirac delta function $\delta(t-t_k)$ used to create the impulsive nature of the thruster torques. The operator $(\dot{\cdot})$ denotes the derivative with respect to time; and the skew-symmetric operator $(\cdot)^\times$ acts on $\boldsymbol{\omega}$, $\boldsymbol{\epsilon}$, and $\boldsymbol{m}$ as follows (shown for a generic vector $\boldsymbol{v}$):

$$\boldsymbol{v}^\times = \begin{bmatrix}0 & -v_3 & v_2\\ v_3 & 0 & -v_1\\ -v_2 & v_1 & 0\end{bmatrix} \tag{28}$$

The disturbance torques, represented by $\boldsymbol{\tau}_{\text{dist}}$ in Eq. (27b), are neglected when designing the controller (consistent with a typical passivity-based approach that treats the disturbances as exogenous inputs), but they are accounted for during the nonlinear simulations used for testing the controller's performance. For near-Earth small spacecraft that are not significantly affected by solar radiation or atmospheric drag, the disturbance sources of importance are the gravity gradient and residual magnetic dipole moments resulting from onboard electronics ([40] Chap. 9):

$$\boldsymbol{\tau}_{\text{dist}} = \frac{3\mu}{|\boldsymbol{r}_B|^5}\boldsymbol{r}_B^\times\boldsymbol{I}\boldsymbol{r}_B + \boldsymbol{m}_{\text{dist}}^\times\boldsymbol{b}_B \tag{29}$$

where $\mu = 3.9859\times10^{14}\ \text{m}^3/\text{s}^2$ for Earth.

The nonlinear differential equations in Eqs. (27a) and (27b) [with the disturbances in Eq. (29)] fully describe the attitude motion of the spacecraft. Numerical integration of this system of equations provides an accurate prediction of the spacecraft's on-orbit attitude changes over time.

IV. Passivity-Based Hybrid Magnetic Attitude Control

The hybrid passivity concepts and conditions described in Sec. II are applied in this section to the specific attitude control problem introduced in Sec. III. Augmenting continuous magnetic actuation with impulsive control provided by thrusters is motivated by a desire to overcome magnetic control's fundamental gain limitation (as demonstrated in [28]) and alleviate its pointwise uncontrollability issues. A design approach that guarantees the closed-loop system's stability using passivity-related concepts is expected to result in improved robustness properties, making the control system better immune to modeling uncertainties and measurement noises.

To design a passivity-based controller, the equations of motion described in Sec. III are linearized in Sec. IV.A, and the resulting state-space model is treated as the plant of the hybrid system considered in Sec. II. The plant's output dynamics are then designed in Sec. IV.B in a manner that satisfies the set of hybrid extended KYP conditions presented in Sec. II.B, hence establishing the passivity of the plant. Finally, aiming to benefit from the hybrid passivity theorem (Theorem 2.2), two strictly passive controller designs are proposed to be used in negative feedback with the passive plant: In Sec. IV.C, the controller is set to provide proportional feedback with constant positive gains; whereas in Sec. IV.D, a dynamic compensator is designed using the hybrid algebraic KYP conditions presented in Sec. II.C.

A. Linearization of the Plant Model

The plant model is obtained by linearizing Eq. (27) (disregarding $\boldsymbol{\tau}_{\text{dist}}$) as follows ([40] Chap. 4):

$$\underbrace{\begin{bmatrix}\dot{\boldsymbol{\theta}}(t)\\ \ddot{\boldsymbol{\theta}}(t)\end{bmatrix}}_{\dot{\boldsymbol{x}}(t)} \approx \underbrace{\begin{bmatrix}\boldsymbol{0}_{3\times3} & \boldsymbol{1}_{3\times3}\\ \boldsymbol{0}_{3\times3} & \boldsymbol{0}_{3\times3}\end{bmatrix}}_{\boldsymbol{A}_c}\underbrace{\begin{bmatrix}\boldsymbol{\theta}(t)\\ \dot{\boldsymbol{\theta}}(t)\end{bmatrix}}_{\boldsymbol{x}(t)} + \underbrace{\begin{bmatrix}\boldsymbol{0}_{3\times3}\\ -\boldsymbol{I}^{-1}\boldsymbol{b}_G^\times(t)\end{bmatrix}}_{B_c(t)}\underbrace{[\boldsymbol{m}(t)]}_{\boldsymbol{u}(t)}, \qquad t \neq t_k \tag{30a}$$

$$\underbrace{\begin{bmatrix}\boldsymbol{\theta}(t_k^+)\\ \dot{\boldsymbol{\theta}}(t_k^+)\end{bmatrix}}_{\boldsymbol{x}(t_k^+)} \approx \underbrace{\begin{bmatrix}\boldsymbol{1}_{3\times3} & \boldsymbol{0}_{3\times3}\\ \boldsymbol{0}_{3\times3} & \boldsymbol{1}_{3\times3}\end{bmatrix}}_{A_d}\underbrace{\begin{bmatrix}\boldsymbol{\theta}(t_k^-)\\ \dot{\boldsymbol{\theta}}(t_k^-)\end{bmatrix}}_{\boldsymbol{x}(t_k^-)} + \underbrace{\begin{bmatrix}\boldsymbol{0}_{3\times3}\\ \boldsymbol{I}^{-1}\end{bmatrix}}_{B_d}\underbrace{[\boldsymbol{n}_k]}_{\boldsymbol{v}_k}, \qquad t = t_k \tag{30b}$$

where Eq. (30a) corresponds to the continuous portion of the hybrid plant $\mathcal{G}^h$, represented by Eq. (1); whereas Eq. (30b) correlates with the discrete portion shown in Eq. (2). This linearization assumes small angles and rates ($\dot{\boldsymbol{\theta}} \approx \boldsymbol{\omega}$ and $\boldsymbol{\theta} \approx 2\boldsymbol{\epsilon}$) and small magnetic dipole moments $\boldsymbol{m}$. It should be noted that, although the linearized model assumes $\boldsymbol{b}_B^\times \approx \boldsymbol{b}_G^\times$ [making use of an identity from [41] that states

$$\boldsymbol{b}_B^\times = (\boldsymbol{C}_{BG}\boldsymbol{b}_G)^\times = \boldsymbol{C}_{BG}\boldsymbol{b}_G^\times\boldsymbol{C}_{GB} \approx (1-\boldsymbol{\theta}^\times)\boldsymbol{b}_G^\times(1+\boldsymbol{\theta}^\times)$$

assuming small angles, and neglecting the resulting $\boldsymbol{\theta}^\times\boldsymbol{\theta}^\times$ term because of its order], the implemented controller will have access to $\boldsymbol{b}_B$ during the mission (via measurements), so the design approach presented in the following sections uses $\boldsymbol{b}_B$ for higher accuracy when computing the matrix $\boldsymbol{B}_c$.

As mentioned earlier, the dynamic compensator proposed in Sec. IV.C relies on the algebraic KYP conditions of Sec. II.C, which presume time-invariant state-space matrices. For this reason, a time-invariant approximate to the system in Eq. (3) is requires. One way of obtaining this involves average the time-varying $\boldsymbol{B}_c(t)\boldsymbol{B}_c^\intercal(t)$ over an orbit (assuming quasi-periodicity of the system with one orbit and, as opposed to averaging $\boldsymbol{B}_c(t)$ itself, which would integrate to 0):

$$\bar{\boldsymbol{B}}_c\bar{\boldsymbol{B}}_c^\intercal = \frac{1}{T}\int_0^T \boldsymbol{B}_c(\tau)\boldsymbol{B}_c^\intercal(\tau)\,\mathrm{d}\tau \tag{31}$$

upon diagonalizing the right-hand side of which an averaged $\bar{\boldsymbol{B}}_c$ can be obtained as follows:

$$\bar{\boldsymbol{B}}_c = \boldsymbol{E}_{nz}\boldsymbol{\Lambda}_{nz}^{1/2} \tag{32}$$

where $\boldsymbol{\Lambda}_{nz}$ contains the nonzero eigenvalues of the right-hand side of Eq. (31) as its diagonal elements, and $\boldsymbol{E}_{nz}$ consists of these eigenvalues' corresponding eigenvectors as its columns. In other words, these matrices are extracted from the diagonalization $\bar{\boldsymbol{B}}_c\bar{\boldsymbol{B}}_c^\intercal = \boldsymbol{E}\boldsymbol{\Lambda}\boldsymbol{E}^{-1}$ that leads to $\boldsymbol{\Lambda} = \text{blockdiag}\{\boldsymbol{\Lambda}_{nz}, \boldsymbol{0}\}$ and $\boldsymbol{E} = [\,\boldsymbol{E}_{nz} \quad \boldsymbol{E}_z\,]$, where $\boldsymbol{E}_z$ has the eigenvectors corresponding to the zero eigenvalues of the right-hand side of Eq. (31) as its columns.

B. Passive Plant Design

As mentioned previously, the idea behind the passivity-based design approach described in this section is to complete the specification of the plant by determining for it appropriate output dynamics, given by Eqs. (1b) and (2b). To this end, assuming full state measurement, some artificial state-space matrices $\boldsymbol{C}_c(t)$, $\boldsymbol{D}_c(t)$, $\boldsymbol{C}_{dk}$, and $\boldsymbol{D}_{dk}$ could be designed such that the set of hybrid KYP conditions provided by Eq. (12) are satisfied, hence establishing the passivity of the plant.

Some simplifying assumptions can be made for the purpose of limiting the design space. Letting $\boldsymbol{W}_c(t) \equiv \boldsymbol{0}$ and $\boldsymbol{W}_{dk} \equiv \boldsymbol{0}$ and assuming a symmetric $\boldsymbol{D}_c$, it follows from Eq. (12c) that $\boldsymbol{D}_c(t) \equiv \boldsymbol{0}$ as well because $\epsilon_{c\kappa} \equiv 0$ for passivity. Furthermore, noting that an inner product of any matrix with itself is positive semidefinite and symmetric, new variables $\boldsymbol{L}_c^\intercal(t)\boldsymbol{L}_c(t) \triangleq \boldsymbol{U}_c(t) \geqslant 0$ and $\boldsymbol{L}_{dk}^\intercal \boldsymbol{L}_{dk} \triangleq \boldsymbol{U}_{dk} \geqslant 0$ are defined. Lastly, setting $\epsilon_{dk} \equiv 0$ for passivity, assuming a symmetric $\boldsymbol{D}_{dk}$, noting the symmetry of $\boldsymbol{P}(t)$ as required by Theorem 2.3, and realizing that $\boldsymbol{A}_{dk} = \boldsymbol{1}$ in Eq. (30b), a simplified and rearranged form of the KYP conditions in Eq. (12) is obtained:

$$\dot{\boldsymbol{P}}(t) = -[\boldsymbol{P}(t)\boldsymbol{A}_c + \boldsymbol{A}_c^\intercal \boldsymbol{P}(t) + \boldsymbol{U}_c(t)] \tag{33a}$$

$$\boldsymbol{P}(t_k^-) = \boldsymbol{P}(t_k^+) + \boldsymbol{U}_{dk} \tag{33b}$$

$$\boldsymbol{C}_c(t) = \boldsymbol{B}_c^\intercal(t)\boldsymbol{P}(t) \tag{33c}$$

$$\boldsymbol{C}_{dk} = \boldsymbol{B}_{dk}^\intercal \boldsymbol{P}(t_k^+) \tag{33d}$$

$$\boldsymbol{D}_{dk} = \frac{1}{2}\boldsymbol{B}_{dk}^\intercal \boldsymbol{P}(t_k^+)\boldsymbol{B}_{dk} \tag{33e}$$

where $\boldsymbol{P}(t)$, $\boldsymbol{U}_c(t)$, and $\boldsymbol{U}_{dk}$ should all be symmetric and positive semidefinite. The matrix $\boldsymbol{P}(t)$ can be determined (numerically, if need be) by integrating Eq. (33a) backward in time and inducing jumps in it at each impulse time using Eq. (33b). To this end, a positive-semidefinite terminal condition $\boldsymbol{P}(t_f)$ is required to be set by the user as a design parameter. With the $\boldsymbol{A}_c$ matrix specific to this problem, defined in Eq. (30a), Eq. (33a) can be rewritten as follows:

$$\begin{aligned}\dot{\boldsymbol{P}}(t) &= -\left(\begin{bmatrix}\boldsymbol{P}_1 & \boldsymbol{P}_2\\ \boldsymbol{P}_2 & \boldsymbol{P}_3\end{bmatrix}\begin{bmatrix}\boldsymbol{0} & \boldsymbol{1}\\ \boldsymbol{0} & \boldsymbol{0}\end{bmatrix} + \begin{bmatrix}\boldsymbol{0} & \boldsymbol{0}\\ \boldsymbol{1} & \boldsymbol{0}\end{bmatrix}\begin{bmatrix}\boldsymbol{P}_1 & \boldsymbol{P}_2\\ \boldsymbol{P}_2 & \boldsymbol{P}_3\end{bmatrix} + \begin{bmatrix}\boldsymbol{U}_{c1} & \boldsymbol{U}_{c2}\\ \boldsymbol{U}_{c2} & \boldsymbol{U}_{c3}\end{bmatrix}\right)\\ &= -\begin{bmatrix}\boldsymbol{U}_{c1} & \boldsymbol{P}_1 + \boldsymbol{U}_{c2}\\ \boldsymbol{P}_1 + \boldsymbol{U}_{c2} & 2\boldsymbol{P}_2 + \boldsymbol{U}_{c3}\end{bmatrix}\end{aligned} \tag{34}$$

Once the Lyapunov solution $\boldsymbol{P}(t)$ is determined, it can be used to assign the control inputs. Two different approaches for doing so are explored in Secs. IV.C and IV.D.

Assume, for simplicity, a constant block-diagonal $\boldsymbol{U}_c$ [as in Eq. (34)], with $\boldsymbol{U}_{c1} = u_{c1}\boldsymbol{1}$, $\boldsymbol{U}_{c2} = \boldsymbol{0}$, and $\boldsymbol{U}_{c3} = u_{c3}\boldsymbol{1}$, where $u_{c1} > 0$ and $u_{c3} > 0$ to ensure positive semidefiniteness. In addition, $\boldsymbol{U}_{dk} \equiv \boldsymbol{0}$ is assumed to keep the Lyapunov solution continuous, even at the impulse times [based on Eq. (33b)]. Integrating Eq. (34) with this choice of $\boldsymbol{U}_c$ yields the following:

$$\dot{\boldsymbol{P}}_1 = -u_{c1}\boldsymbol{1} \Rightarrow \boldsymbol{P}_1 = -u_{c1}t\boldsymbol{1} + \boldsymbol{C}_1 \tag{35a}$$

$$\dot{\boldsymbol{P}}_2 = u_{c1}t\boldsymbol{1} - \boldsymbol{C}_1 \Rightarrow \boldsymbol{P}_2 = \frac{u_{c1}}{2}t^2\boldsymbol{1} - t\boldsymbol{C}_1 + \boldsymbol{C}_2 \tag{35b}$$

$$\begin{aligned}\dot{\boldsymbol{P}}_3 &= -u_{c1}t^2\boldsymbol{1} + 2t\boldsymbol{C}_1 - 2\boldsymbol{C}_2 - u_{c3}\boldsymbol{1} \Rightarrow \boldsymbol{P}_3\\ &= -\frac{u_{c1}}{3}t^3\boldsymbol{1} + t^2\boldsymbol{C}_1 - 2t\boldsymbol{C}_2 - u_{c3}t\boldsymbol{1} + \boldsymbol{C}_3\end{aligned} \tag{35c}$$

where the constants of integration can be solved for by assuming a terminal condition of $\boldsymbol{P}(t_f)$:

$$\boldsymbol{P}_1 = \boldsymbol{P}_1(t_f) + u_{c1}(t_f - t)\boldsymbol{1} \tag{36a}$$

$$\boldsymbol{P}_2 = \boldsymbol{P}_2(t_f) + (t_f - t)\boldsymbol{P}_1(t_f) + \frac{u_{c1}}{2}(t_f - t)^2\boldsymbol{1} \tag{36b}$$

$$\begin{aligned}\boldsymbol{P}_3 &= \boldsymbol{P}_3(t_f) + 2(t_f - t)\boldsymbol{P}_2(t_f) + (t_f - t)^2\boldsymbol{P}_1(t_f) + \frac{u_{c1}}{3}(t_f - t)^3\boldsymbol{1}\\ &\quad + u_{c3}(t_f - t)\boldsymbol{1}\end{aligned} \tag{36c}$$

which shows a linear, quadratic, and cubic increase (moving backward from $t = t_f$) in $\boldsymbol{P}_1$, $\boldsymbol{P}_2$, and $\boldsymbol{P}_3$, respectively. This becomes problematic when t_f is large because the initial values of $\boldsymbol{P}(t)$ diverge to infinity, rendering the controller useless. To remedy this problem, this plant design procedure also incorporates resetting of the Lyapunov solution, at the end of every orbit, to its terminal value: i.e., $\boldsymbol{P}(iT) = \boldsymbol{P}(t_f) = \boldsymbol{P}_f$, $i \in \mathbb{N}$. The Lyapunov solution provided in Eq. (36) then takes the following piecewise form for $i \in \mathbb{N}$:

$$\begin{aligned}&\boldsymbol{P}_1 = \boldsymbol{P}_{1f} + u_{c1}(iT - t)\boldsymbol{1}, \quad t \in [(i-1)T, iT)\\ &\boldsymbol{P}_2 = \boldsymbol{P}_{2f} + (iT - t)\boldsymbol{P}_{1f} + \frac{u_{c1}}{2}(iT - t)^2\boldsymbol{1}, \quad t \in [(i-1)T, iT)\\ &\boldsymbol{P}_3 = \boldsymbol{P}_{3f} + 2(iT - t)\boldsymbol{P}_{2f} + (iT - t)^2\boldsymbol{P}_{1f} + \frac{u_{c1}}{3}(iT - t)^3\boldsymbol{1} + u_{c3}(iT - t)\boldsymbol{1},\\ &\quad t \in [(i-1)T, iT)\end{aligned} \tag{37}$$

This is an analytic solution that does not require numerical backward integration, owing to the choice of a constant $\boldsymbol{U}_c$. In theory, the terminal conditions can be set to any $\boldsymbol{P}(t_f) \geqslant 0$; in practice, however, setting it to $\boldsymbol{0}$ can entail unsatisfactory steady-state performance resulting from loss of control at the end of each orbit. Larger terminal values are therefore recommended, and they are used in the simulations presented in Sec. V.

When simulating the nonlinear dynamics in Eq. (27) [together with the disturbance torques in Eq. (29)], starting with some initial conditions at time zero, the analytic Lyapunov solution $\boldsymbol{P}(t)$ and its value immediately before each impulse are used to compute, using the approaches described in Secs. IV.C and IV.D, the magnetic dipole moments and thruster gains (outputs of a strictly passive feedback controller) that guarantee the system's linear stability under the influence of sufficiently small disturbances.

What remains is designing the controller and determining the control inputs of the plant. Based on Theorem 2.3, any input strictly passive controller would render the closed-loop system (with the passive plant of Sec. IV.B) stable in the presence of sufficiently small disturbances. In Secs. IV.C and IV.D, two different design approaches for the controller are presented.

C. Input Strictly Passive Constant-Gain Controller

In this design, a proportional output feedback controller with constant positive gains is chosen to satisfy the strict passivity condition, considering the negative feedback interconnection of Fig. 1 (with $\boldsymbol{d} = \boldsymbol{0}$):

$$\boldsymbol{u}_c(t) = -\hat{\boldsymbol{y}}_c(t) = -k_c\boldsymbol{y}_c(t) \tag{38a}$$

$$\boldsymbol{u}_{dk} = -\hat{\boldsymbol{y}}_{dk} = -k_d\boldsymbol{y}_{dk} \tag{38b}$$

where $\boldsymbol{y}_c(t)$ and $\boldsymbol{y}_{dk}$ are the plant outputs, represented by Eqs. (1b) and (2b), respectively. Recalling the assumption that $\boldsymbol{D}_c(t) \equiv \boldsymbol{0}$ and using Eqs. (33c–33e) for the plant, one obtains the following:

$$\boldsymbol{u}_c(t) = -k_c[\boldsymbol{B}_c^\intercal(t)\boldsymbol{P}(t)\boldsymbol{x}(t)] \tag{39a}$$

$$\boldsymbol{u}_{dk} = -k_d\left[\boldsymbol{B}_{dk}^{\mathsf{T}}\boldsymbol{P}(t_k^+)\boldsymbol{x}(t_k^-) + \frac{1}{2}\boldsymbol{B}_{dk}^{\mathsf{T}}\boldsymbol{P}(t_k^+)\boldsymbol{B}_{dk}\boldsymbol{u}_{dk}\right] \tag{39b}$$

Lastly, using the block-diagonal form of $\boldsymbol{P}$ introduced in Eq. (34) and the $\boldsymbol{B}_c(t)$ and $\boldsymbol{B}_{dk}$ matrices specific to this problem [defined in Eq. (30)], the control inputs can be solved for from Eq. (39):

$$\boldsymbol{u}_c(t) = -k_c\boldsymbol{b}_B^{\times}(t)\boldsymbol{I}^{-1}[\boldsymbol{P}_2(t)\boldsymbol{\theta}(t) + \boldsymbol{P}_3(t)\dot{\boldsymbol{\theta}}(t)] \tag{40a}$$

$$\boldsymbol{u}_{dk} = -k_d\left[\boldsymbol{1} + \frac{k_d}{2}I^{-1}\boldsymbol{P}_3(t_k^+)\boldsymbol{I}^{-1}\right]^{-1}\boldsymbol{I}^{-1}[\boldsymbol{P}_2(t_k^+)\boldsymbol{\theta}(t_k^-) + \boldsymbol{P}_3(t_k^+)\dot{\boldsymbol{\theta}}(t_k^-)] \tag{40b}$$

where a symmetric moment of inertia matrix $\boldsymbol{I}$ is also assumed. The control inputs provided by Eq. (40) are computed using the Lyapunov solution $\boldsymbol{P}(t)$, an analytic solution of which was obtained in Sec. IV.B upon assuming constant $\boldsymbol{U}_c$ and $\boldsymbol{U}_d$ matrices.

D. Input Strictly Passive Dynamic Compensator

Analogously to the hybrid linear system represented by Eqs. (1) and (2), we define a hybrid dynamic compensator structure for the controller $\mathscr{H}^h$, the input of which is the plant's output. For simplicity, an LTI system is adopted for this controller:

The continuous-time portion of $\mathscr{H}^h$ at $t \neq t_k$ is given, with the initial condition $\hat{\boldsymbol{x}}(t_0)$ (set to $\boldsymbol{0}$ in the absence of any other justifiable value) by

$$\dot{\hat{\boldsymbol{x}}}(t) = \hat{\boldsymbol{A}}_c\hat{\boldsymbol{x}}(t) + \hat{\boldsymbol{B}}_c\hat{\boldsymbol{u}}_c(t) \tag{41a}$$

$$\hat{\boldsymbol{y}}_c(t) = \hat{\boldsymbol{C}}_c\hat{\boldsymbol{x}}(t) + \hat{\boldsymbol{D}}_c\hat{\boldsymbol{u}}_c(t) \tag{41b}$$

whereas the discrete-time portion of $\mathscr{H}^h$ at $t = t_k$ is given by

$$\hat{\boldsymbol{x}}(t_k^+) = \hat{\boldsymbol{A}}_d\hat{\boldsymbol{x}}(t_k^-) + \hat{\boldsymbol{B}}_d\hat{\boldsymbol{u}}_{dk} \tag{42a}$$

$$\hat{\boldsymbol{y}}_{dk} = \hat{\boldsymbol{C}}_d\hat{\boldsymbol{x}}(t_k^-) + \hat{\boldsymbol{D}}_d\hat{\boldsymbol{u}}_{dk} \tag{42b}$$

where $\hat{\boldsymbol{x}}(t)$:$\mathbb{R}^+ \to \mathbb{R}^{n\times 1}$ is the controller's "state" and has no physical significance. The vectors $\hat{\boldsymbol{u}}_c(t)$:$\mathbb{R}^+ \to \mathbb{R}^{m_c\times 1}$ and $\hat{\boldsymbol{u}}_{dk}$:$\mathbb{N} \to \mathbb{R}^{m_d\times 1}$ are the inputs used by the controller [that, for the negative feedback structure of Fig. 1 with $\boldsymbol{d} = \boldsymbol{0}$, correspond to the plant's outputs, i.e., $\hat{\boldsymbol{u}}_c(t) = \boldsymbol{y}_c(t)$ and $\hat{\boldsymbol{u}}_{dk} = \boldsymbol{y}_{dk}$] and, assuming equal input/output dimensions, $\hat{\boldsymbol{y}}_c(t)$:$\mathbb{R}^+ \to \mathbb{R}^{m_c\times 1}$ and $\hat{\boldsymbol{y}}_{dk}$:$\mathbb{N} \to \mathbb{R}^{m_d\times 1}$ are the controller's output vectors [that for Fig. 1, correspond to the negative of the plant's control inputs, i.e., $\hat{\boldsymbol{y}}_c(t) = -\boldsymbol{u}_c(t)$ and $\hat{\boldsymbol{y}}_{dk} = -\boldsymbol{u}_{dk}$]. The constant continuous-time matrices $\hat{\boldsymbol{A}}_c$, $\hat{\boldsymbol{B}}_c$, $\hat{\boldsymbol{C}}_c$, and $\hat{\boldsymbol{D}}_c$, as well as the discrete-time $\hat{\boldsymbol{A}}_d$, $\hat{\boldsymbol{B}}_d$, $\hat{\boldsymbol{C}}_d$, and $\hat{\boldsymbol{D}}_d$, are all dimensioned appropriately, in the same way as their plant analog.

Making use of the aforementioned plant–controller relationships arising from the negative feedback loop of Fig. 1 (with $\boldsymbol{d} = \boldsymbol{0}$), the evolution of the controller's state based on Eqs. (41a) and (42a) is dictated by

$$\dot{\hat{\boldsymbol{x}}}(t) = \hat{\boldsymbol{A}}_c\hat{\boldsymbol{x}}(t) + \hat{\boldsymbol{B}}_c\hat{\boldsymbol{y}}_c(t), \qquad t \neq t_k \tag{43a}$$

$$\hat{\boldsymbol{x}}(t_k^+) = \hat{\boldsymbol{A}}_d\hat{\boldsymbol{x}}(t_k^-) + \hat{\boldsymbol{B}}_d\boldsymbol{y}_{dk}, \qquad t = t_k \tag{43b}$$

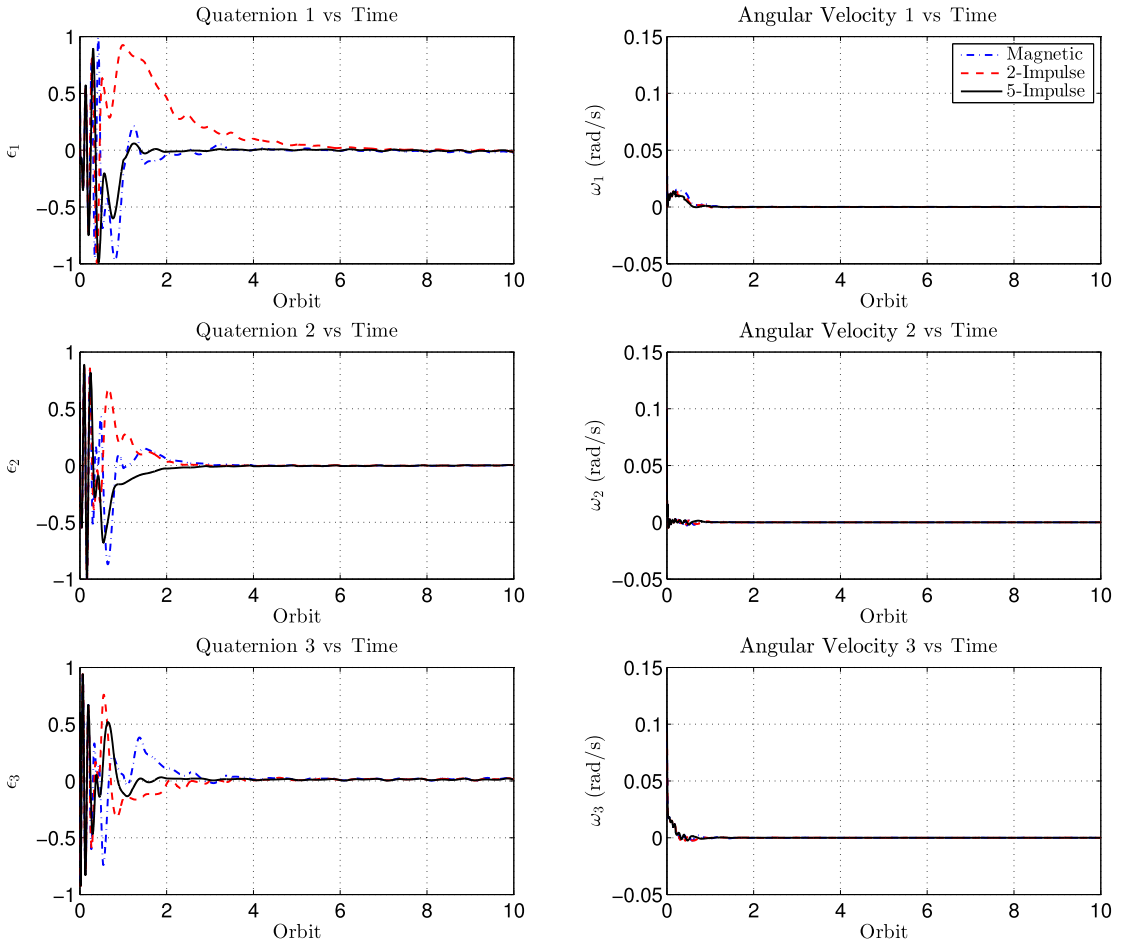

Fig. 2 Transient performance of constant-gain controller, with quaternions and angular velocity: passivity-based five-impulse hybrid (solid lines), two-impulse hybrid (dashed lines), and solely magnetic (dashed–dotted lines).

whereas the continuous- and discrete-time control inputs to be fed back to the plant are provided by

$$\boldsymbol{u}_c(t) = -\hat{\boldsymbol{C}}_c\hat{\boldsymbol{x}}(t) - \hat{\boldsymbol{D}}_c\boldsymbol{y}_c(t) \tag{44a}$$

$$\boldsymbol{u}_{dk} = -\hat{\boldsymbol{C}}_d\hat{\boldsymbol{x}}(t_k^-) - \hat{\boldsymbol{D}}_d\boldsymbol{y}_{dk} \tag{44b}$$

What remains is determining the matrices such that the resulting dynamic compensator is input strictly passive. A possible design approach that yields satisfactory performance follows, but the reader should keep in mind that many other approaches may be possible and should be explored as part of future work on this topic.

We select $\hat{\boldsymbol{C}}_c = \boldsymbol{R}_c^{-1}\bar{\boldsymbol{B}}_c^{\intercal}\bar{\boldsymbol{X}}$, where $\bar{\boldsymbol{B}}_c$ is the time-invariant equivalent [given by Eq. (32)] of the plant's $\boldsymbol{B}_c(t)$ matrix, based on the solution $\bar{\boldsymbol{X}}$ of the familiar linear quadratic regulator problem that minimizes the following:

$$J = \frac{1}{2}\int_0^\infty [\boldsymbol{x}^{\intercal}(\tau)\boldsymbol{Q}_c\boldsymbol{x}(\tau) + \boldsymbol{u}_c^{\intercal}(\tau)\boldsymbol{R}_c\boldsymbol{u}_c(\tau)]\,\mathrm{d}\tau \tag{45}$$

where $\boldsymbol{Q}_c = \boldsymbol{Q}_c^{\intercal} > 0$ and $\boldsymbol{R}_c = \boldsymbol{R}_c^{\intercal} > 0$ are user-defined penalty matrices. The solution is provided by solving the following continuous-time algebraic Riccati equation for $\bar{\boldsymbol{X}}$:

$$\boldsymbol{A}_c^{\intercal}\bar{\boldsymbol{X}} + \bar{\boldsymbol{X}}\boldsymbol{A}_c - \bar{\boldsymbol{X}}\boldsymbol{B}_c\boldsymbol{R}_c^{-1}\boldsymbol{B}_c^{\intercal}\bar{\boldsymbol{X}} + \boldsymbol{Q}_c = \boldsymbol{0} \tag{46}$$

where $\boldsymbol{A}_c$ of the plant [given by Eq. (30a)] is constant in this problem. We then let

$$\hat{\boldsymbol{A}}_c = \boldsymbol{A}_c - \bar{\boldsymbol{B}}_c\hat{\boldsymbol{C}}_c = \boldsymbol{A}_c - \bar{\boldsymbol{B}}_c\boldsymbol{R}_c^{-1}\bar{\boldsymbol{B}}_c^{\intercal}\bar{\boldsymbol{X}}$$

which is guaranteed to have eigenvalues with negative real parts. With $\hat{\boldsymbol{A}}_c$ and $\hat{\boldsymbol{C}}_c$ determined, the remaining continuous-time matrices to design are $\hat{\boldsymbol{B}}_c$ and $\hat{\boldsymbol{D}}_c$. This is where input strict passivity comes in, and the set of hybrid algebraic KYP conditions of Sec. II.C are used (as the controller's system is LTI): Let (similar to the plant's design in Sec. IV.B) $\boldsymbol{W}_c \equiv \boldsymbol{0}$ and $\boldsymbol{L}_c^{\intercal}\boldsymbol{L}_c \equiv \boldsymbol{V}_c \geqslant 0$. The algebraic Lyapunov solution is obtained via Eq. (26a) using the controller's state-space matrices:

$$\hat{\boldsymbol{A}}_c^{\intercal}\bar{\boldsymbol{P}} + \bar{\boldsymbol{P}}\hat{\boldsymbol{A}}_c = -\boldsymbol{V}_c \tag{47}$$

where $\boldsymbol{V}_c$ is a design parameter specified by the user. Once $\bar{\boldsymbol{P}}$ is solved for, it can be used in Eq. (26b) (with $\boldsymbol{W}_c \equiv \boldsymbol{0}$) to determine $\hat{\boldsymbol{B}}_c = \bar{\boldsymbol{P}}^{-1}\hat{\boldsymbol{C}}_c^{\intercal} = \bar{\boldsymbol{P}}^{-1}(\boldsymbol{R}_c^{-1}\bar{\boldsymbol{B}}_c^{\intercal}\bar{\boldsymbol{X}})^{\intercal}$. Lastly, assuming a symmetric $\boldsymbol{D}_c$, from Eq. (26c) we obtain $\hat{\boldsymbol{D}}_c = \epsilon_c\boldsymbol{1}$, which completes the specification of the continuous-time portion of the hybrid controller in a manner that, thus far, satisfies the pertinent portion of the hybrid algebraic KYP conditions by construction.

Before proceeding with the discrete-time matrices, we assume (similar to the continuous-time case) that $\boldsymbol{W}_d \equiv \boldsymbol{0}$, and we let $\boldsymbol{L}_d^{\intercal}\boldsymbol{L}_d \triangleq \boldsymbol{V}_d \geqslant 0$. Because the set of conditions in Eq. (26) requires the same $\bar{\boldsymbol{P}}$ for both continuous- and discrete-time portions, we let $\hat{\boldsymbol{A}}_d = a_d\boldsymbol{1}$, $a_d \leqslant 1$, which is guaranteed to satisfy Eq. (26a):

$$\hat{\boldsymbol{A}}_d^{\intercal}\bar{\boldsymbol{P}}\hat{\boldsymbol{A}}_d - \bar{\boldsymbol{P}} = -\boldsymbol{V}_d \tag{48}$$

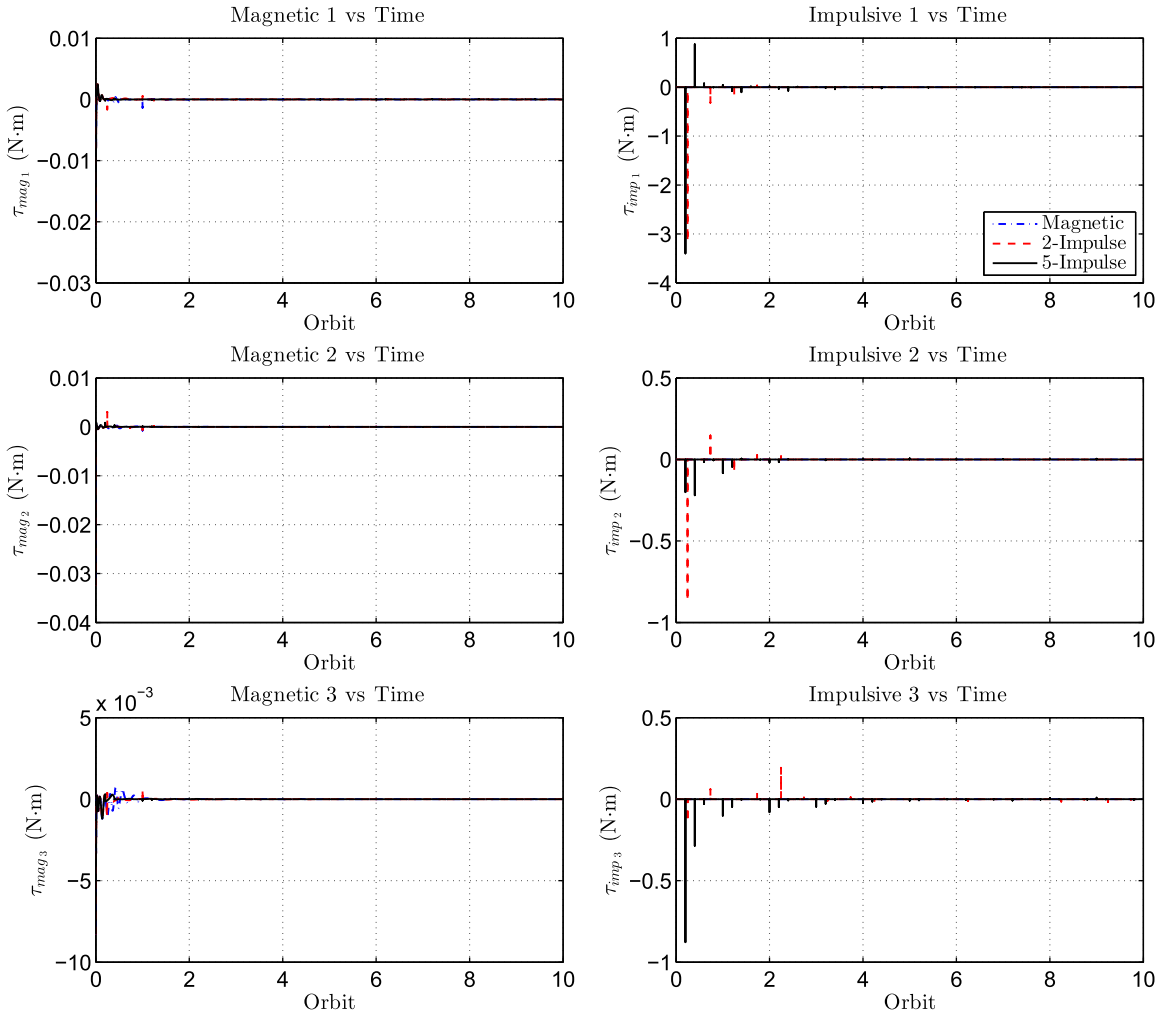

Fig. 3 Transient performance of constant-gain controller, with continuous and impulsive torques: passivity-based five-impulse hybrid (solid lines), two-impulse hybrid (dashed lines), and solely magnetic (dashed–dotted lines).

for some positive-semidefinite $\boldsymbol{V}_d$. Inspired by the form of the plant's $\boldsymbol{B}_d$ matrix, we then choose $\hat{\boldsymbol{B}}_d = b_d[\mathbf{0} \quad \mathbf{1}]^\intercal$, and we determine $\hat{\boldsymbol{C}}_d = \hat{\boldsymbol{B}}_d^\intercal \bar{\boldsymbol{P}} \hat{\boldsymbol{A}}_d$ using Eq. (26e) (with $\boldsymbol{W}_d \equiv \mathbf{0}$). Finally, assuming a symmetric $\hat{\boldsymbol{D}}_d$ similar to its continuous-time counterpart, from Eq. (26f), we have $\hat{\boldsymbol{D}}_d = \epsilon_d \mathbf{1} + (1/2)\hat{\boldsymbol{B}}_d^\intercal \bar{\boldsymbol{P}} \hat{\boldsymbol{B}}_d$, which completes the discrete-time portion's design.

The control inputs to be fed back to the controller can now be evaluated at each time instance using Eq. (44). Substituting the matrices selected in this paper into that equation yields

$$\boldsymbol{u}_c(t) = -\boldsymbol{R}_c^{-1} \bar{\boldsymbol{B}}_c^\intercal \bar{\boldsymbol{X}} \hat{\boldsymbol{x}}(t) - \epsilon_c \boldsymbol{y}_c(t) \tag{49a}$$

$$\boldsymbol{u}_{dk} = -a_d b_d [\bar{\boldsymbol{P}}_2 \quad \bar{\boldsymbol{P}}_3] \hat{\boldsymbol{x}}(t_k^-) - (\epsilon_d \mathbf{1} + b_d^2 \bar{\boldsymbol{P}}_3) \boldsymbol{y}_{dk} \tag{49b}$$

where $\bar{\boldsymbol{X}}$ and $\bar{\boldsymbol{P}}$ [partitioned in a block-diagonal form similar to $\boldsymbol{P}(t)$ in Eq. (34)] are the solutions of the algebraic Riccati and Lyapunov equations in Eqs. (46) and (47), respectively. The evolution of the state variable $\hat{\boldsymbol{x}}(t)$ is governed by Eq. (43):

$$\dot{\hat{\boldsymbol{x}}}(t) = (\boldsymbol{A}_c - \bar{\boldsymbol{B}}_c \boldsymbol{R}_c^{-1} \bar{\boldsymbol{B}}_c^\intercal \bar{\boldsymbol{X}}) \hat{\boldsymbol{x}}(t) + (\bar{\boldsymbol{P}}^{-1} \bar{\boldsymbol{X}}^\intercal \bar{\boldsymbol{B}}_c \boldsymbol{R}_c^{-1}) \boldsymbol{y}_c(t), \qquad t \neq t_k \tag{50a}$$

$$\hat{\boldsymbol{x}}(t_k^+) = a_d \hat{\boldsymbol{x}}(t_k^-) + b_d [\mathbf{0} \quad \mathbf{1}]^\intercal \boldsymbol{y}_{dk}, \qquad t = t_k \tag{50b}$$

Having satisfied all of the hybrid algebraic KYP conditions of Theorem 2.4 by construction of the matrices, the proposed hybrid dynamic compensator is guaranteed to be input strictly passive (in a linear sense), and its negative feedback interconnection with the passive plant of Sec. IV.B should be stable, according to Theorem 2.2.

V. Numerical Examples

Simulations are performed using MATLAB® to study the performance of the proposed passivity-based hybrid magnetic attitude controller. A circular near-polar Keplerian orbit with orbital parameters

$$\{a, e, i, \Omega, \omega, t_0\} = \{6.82 \times 10^6 \text{ m}, 0, 87 \text{ deg}, 0 \text{ deg}, 0 \text{ deg}, 0 \text{ s}\}$$

is assumed, corresponding to an altitude of 450 km. The moment of inertia matrix of the spacecraft is set to $\boldsymbol{I} = \text{diag}\{27, 17, 25\}$ kg · m^2; based on some missions considered in [19], the spacecraft is assumed to be equipped with three magnetic torquers with $R = 100\ \Omega$, $c = 1000$ turns, $d = 25$ cm, and $A = d^2$ (assuming square coils).

Numerical integration is performed on the full nonlinear equations of motion given in Eq. (27) using a fourth-order Runge–Kutta algorithm. At each time step, the linearized model of Eq. (30) is constructed based on an estimation of the magnetic field vector; because the design approach of Sec. IV.B provides an analytic Lyapunov solution $\boldsymbol{P}(t)$, the plant's desired measurement matrices are readily obtained. Then, depending on which type of controller is being used, the control inputs are computed at every time instance from either Eq. (40), for the constant-gain controller, or from Eqs. (49) and (50), for the dynamic compensator. In conjunction with the gravity gradient and residual magnetic dipole moments (set to $\boldsymbol{m}_{\text{dist}} = [0.1\ 0.1\ 0.1]^\intercal$ A · m^2) disturbance torques, these control

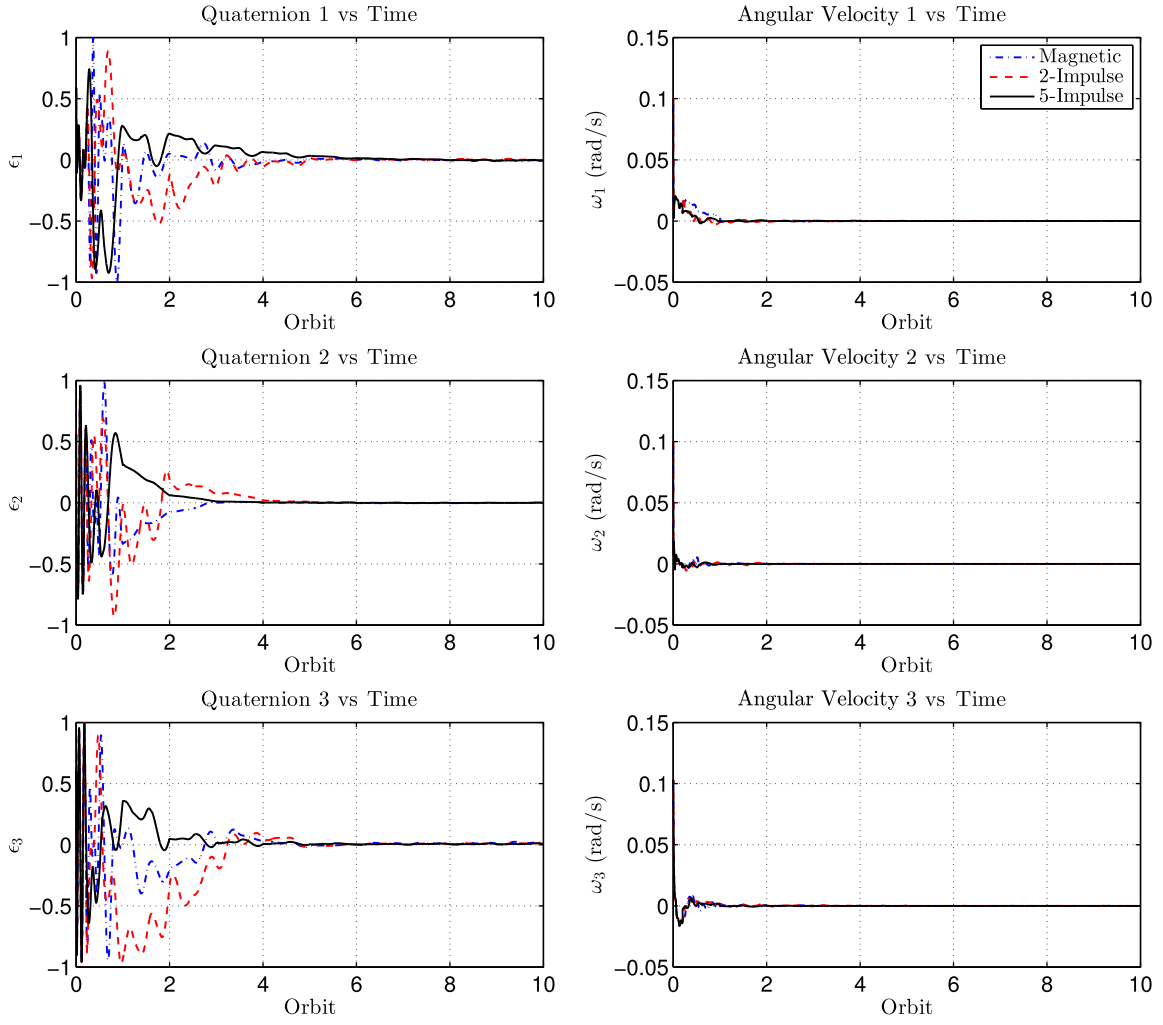

Fig. 4 Transient performance of dynamic compensator, with quaternions and angular velocity: passivity-based five-impulse hybrid (solid lines), two-impulse hybrid (dashed lines), and solely magnetic (dashed–dotted lines).

torques are applied and the resulting nonlinear states are obtained from Eq. (27).

For the plant, the design approach presented in Sec. IV.B is used. Following that approach, the discrete-time $\boldsymbol{U}_{dk}$ is set to $\boldsymbol{0}$, producing a continuous Lyapunov solution. A constant block-diagonal form is assumed for $\boldsymbol{U}_c = \text{blockdiag}\{u_{c1}\boldsymbol{1}_{3\times3}, u_{c3}\boldsymbol{1}_{3\times3}\}$, and the scalar parameters are tuned to be $u_{c1} = 0.3$ and $u_{c3} = 100$. To prevent $\boldsymbol{P}(t)$ from growing (backward) without bound, the solution is reset at every orbital period; and to prevent loss of control as a result of its zero or small values, the terminal value to which the solution is reset at every orbit is set to $\boldsymbol{P}_1(iT) = \boldsymbol{0}_{3\times3}$, $\boldsymbol{P}_2(iT) = 2\times10^6\boldsymbol{1}_{3\times3}$, and $\boldsymbol{P}_3(iT) = 2\times10^9\boldsymbol{1}_{3\times3}$. Two types of hybrid controller are used: a two-impulse one with thrusts applied at $t_{2k-1} = 0.245 + (k-1)T$, $t_{2k} = 0.735T + (k-1)T$, $k \in \{1, 2, \ldots, 10\}$ (which correspond to the times at which the magnetic controller has the least control authority [36]); and a five-impulse controller with an equally spaced set of impulse times (separated by $0.20T$ and starting from time $0.20T$), namely, at $t_k = k\times0.20T$, $k \in \{1, 2, \ldots, 10\times5\}$ for 10 orbits.

For the constant-gain controller of Sec. IV.C, matrix $\boldsymbol{U}_c$ in Eq. (33a) is set constructed using $u_{c1} = 0.3$ and $u_{c3} = 100$, and the continuous and impulsive control gains used in Eq. (40) are set to $k_c = 0.5$ and $k_d = 5\times10^{-8}$, respectively. For the dynamic compensator proposed in Sec. IV.D, the penalty matrices used in the algebraic Riccati equation, given by Eq. (46), are set to $\boldsymbol{Q}_c = q_c\boldsymbol{1}_{6\times6}$ and $\boldsymbol{R}_c = r_c\boldsymbol{1}_{3\times3}$, with $q_c = 8\times10^5$ and $r_c = 10^4$. In addition, $\boldsymbol{V}_c = v_c\boldsymbol{1}_{6\times6}$ is used for the algebraic Lyapunov equation, given by Eq. (47), with the scaling factor tuned to $v_c = 5\times10^2$. Lastly, for the assumed forms of $\hat{\boldsymbol{A}}_d = a_d\boldsymbol{1}_{6\times6}$ and $\hat{\boldsymbol{B}}_d = b_d[\boldsymbol{0}_{3\times3} \quad \boldsymbol{1}_{3\times3}]^\intercal$, the parameters are set to $a_d = -0.2$ and $b_d = 2\times10^{-9}$, and the positive parameters used to ensure input strict passivity via the conditions in Eqs. (26c) and (26f) are tuned to $\epsilon_c = 0.5$ and $\epsilon_d = 10^{-9}$. These parameters, together with the algebraic Riccati and Lyapunov solutions ($\bar{\boldsymbol{X}}$ and $\bar{\boldsymbol{P}}$), are used to compute the control inputs via Eqs. (49) and (50).

As a means of comparison and to assess the effectiveness of a hybrid architecture, a solely magnetic controller is also designed and tested using similar, but continuous only, passivity-based approaches (with no impulses applied). To this end, the same $\boldsymbol{P}(t)$ from Eq. (37) is used for the plant, but only in conjunction with Eq. (40a) (for the constant-gain controller) or Eqs. (49a) and (50a) (for the dynamic compensator), without a need for their discrete-time counterparts in Eq. (40b) or Eqs. (49b) and (50b). Similar to the hybrid controllers, and in order to allow for a meaningful performance comparison, the same continuous parameters are used, namely, $u_{c1} = 0.3$ and $u_{c3} = 100$ for the plant, and $k_c = 0.5$ (for the solely magnetic constant-gain controller) or $q_c = 8\times10^5$, $r_c = 10^4$, $v_c = 5\times10^2$, and (for the solely magnetic dynamic compensator).

A. Transient Performance

The initial conditions are first set to $\boldsymbol{\epsilon}_0 = [0.50 \quad 0.50 \quad 0.50]^\intercal$, $\eta_0 = 0.50$, and $\boldsymbol{\omega}_0 = [0.50 \quad 0.50 \quad 0.50]^\intercal$ rad/s. Figures 2 and 3 depict the nonlinear simulation results over 10 orbits using the passivity-based hybrid constant-gain controller presented in Sec. IV.C, whereas Figs. 4 and 5 show those obtained using the passivity-based hybrid dynamic compensator proposed in Sec. IV.D. For both control schemes, the included cases are five-impulse hybrid (solid curves), two-impulse hybrid (dashed curves), and solely magnetic (dashed–dotted curves) control. The quaternions and angular velocity results in Figs. 2 and 4 demonstrate the satisfactory performance of both of the proposed passivity-based control schemes, with their respective control torques shown in Figs. 3 and 5.

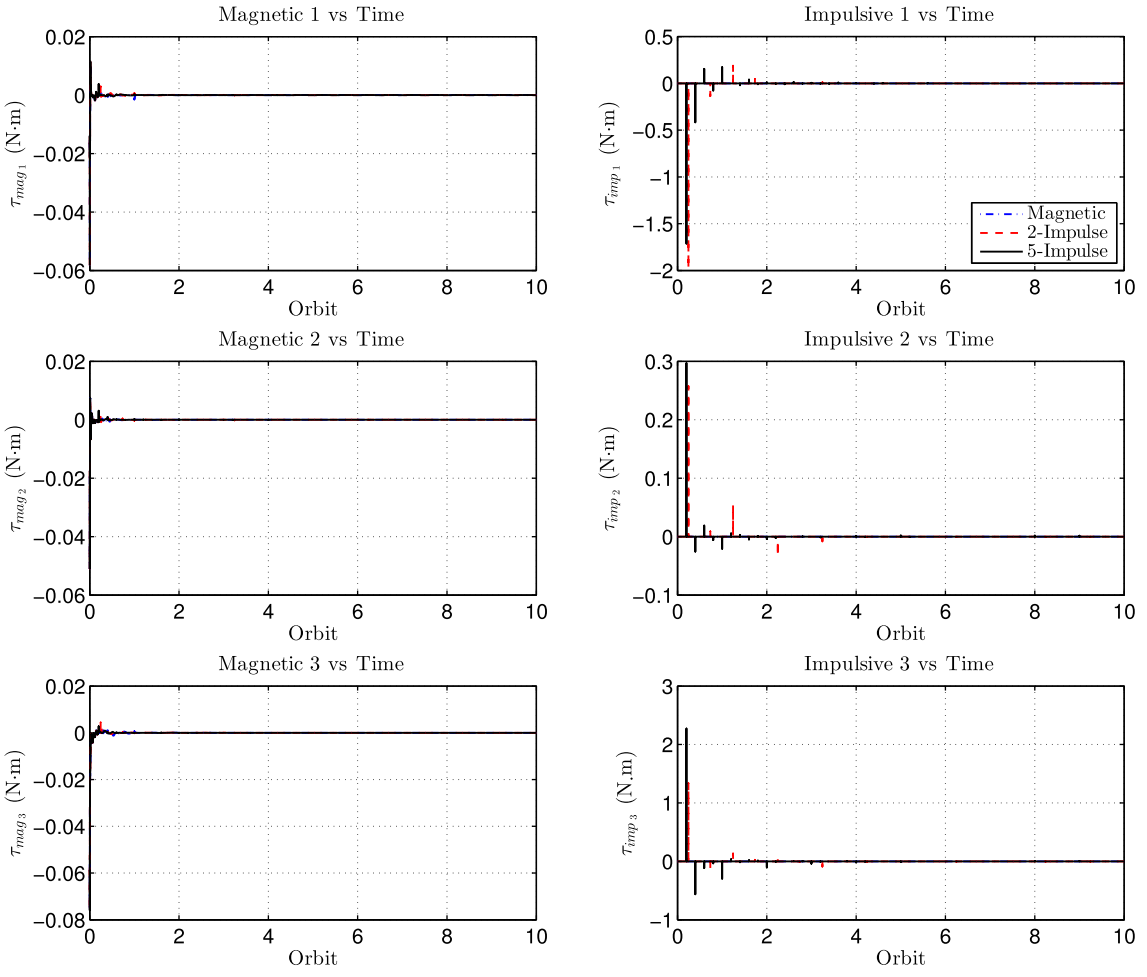

Fig. 5 Transient performance of dynamic compensator, with continuous and impulsive torques: passivity-based five-impulse hybrid (solid lines), two-impulse hybrid (dashed lines), and solely magnetic (dashed–dotted lines).

Table 1 Transient performance of reference PD (based on [28]) vs magnetic, two-impulse, and five-impulse constant-gain controllers over $10T$

Parameter	Description	Reference PD	Magnetic	Two-impulse	Five-impulse	Unit
E_{10T}	Electrical energy usage	5.08×10^{1}	2.37×10^{1}	2.37×10^{1}	2.36×10^{1}	MJ
$\|\boldsymbol{\tau}_c\|_{10T}$	Magnetic torque norm	2.70×10^{-3}	1.85×10^{-3}	1.85×10^{-3}	1.85×10^{-3}	N · m
$\|\boldsymbol{\tau}_d\|_{10T}$	Impulsive torque norm	0	0	1.80×10^{-3}	2.12×10^{-3}	N · m
$\|\boldsymbol{\omega}\|_{10T}$	Angular velocity norm	9.34×10^{-3}	5.02×10^{-3}	4.72×10^{-3}	4.59×10^{-3}	rad/s
$\|\boldsymbol{\phi}\|_{10T}$	Rotation angle norm	2.45×10^{0}	7.78×10^{-1}	9.21×10^{-1}	6.22×10^{-1}	rad

Table 2 Transient performance of reference PD (based on [28]) vs magnetic, two-impulse, and five-impulse dynamic compensators over $10T$

Parameter	Description	Reference PD	Magnetic	Two-impulse	Five-impulse	Unit
E_{10T}	Electrical energy usage	5.08×10^{1}	2.61×10^{1}	2.61×10^{1}	2.61×10^{1}	MJ
$\|\boldsymbol{\tau}_c\|_{10T}$	Magnetic torque norm	2.70×10^{-3}	1.91×10^{-3}	1.90×10^{-3}	1.90×10^{-3}	N · m
$\|\boldsymbol{\tau}_d\|_{10T}$	Impulsive torque norm	0	0	3.24×10^{-3}	3.98×10^{-3}	N · m
$\|\boldsymbol{\omega}\|_{10T}$	Angular velocity norm	9.34×10^{-3}	5.48×10^{-3}	4.92×10^{-3}	4.65×10^{-3}	rad/s
$\|\boldsymbol{\phi}\|_{10T}$	Rotation angle norm	2.45×10^{0}	7.50×10^{-1}	1.07×10^{0}	6.90×10^{-1}	rad

In both cases, the five-impulse hybrid controller generally outperforms the solely magnetic and the two-impulse ones, as is further evident from Tables 1 and 2, which present some quantitative norms computed over 10 orbits. These measures include the electrical energy estimated using

$$E_{10T} = 3R/(c^2A^2) \int_0^{10T} \boldsymbol{m}^\intercal \boldsymbol{m} \, \mathrm{d}t$$

as well as some root-mean-square-like norms defined generically as

$$\|\boldsymbol{v}\|_{10T} \triangleq \sqrt{\left(\int_0^{10T} \boldsymbol{v}^\intercal \boldsymbol{v} \, \mathrm{d}t \right) / (10T)}$$

such that $\boldsymbol{v}$ is set to $\boldsymbol{\tau}_c = \boldsymbol{m}^{\times} \boldsymbol{b}_B$ for magnetic torques measure, is set to $\boldsymbol{\omega}$ for a measure of angular velocities, and is set to $\boldsymbol{\phi}$ for rotation angles. To compute the angle $\boldsymbol{\phi}$ from Euler's axis/angle parameters,

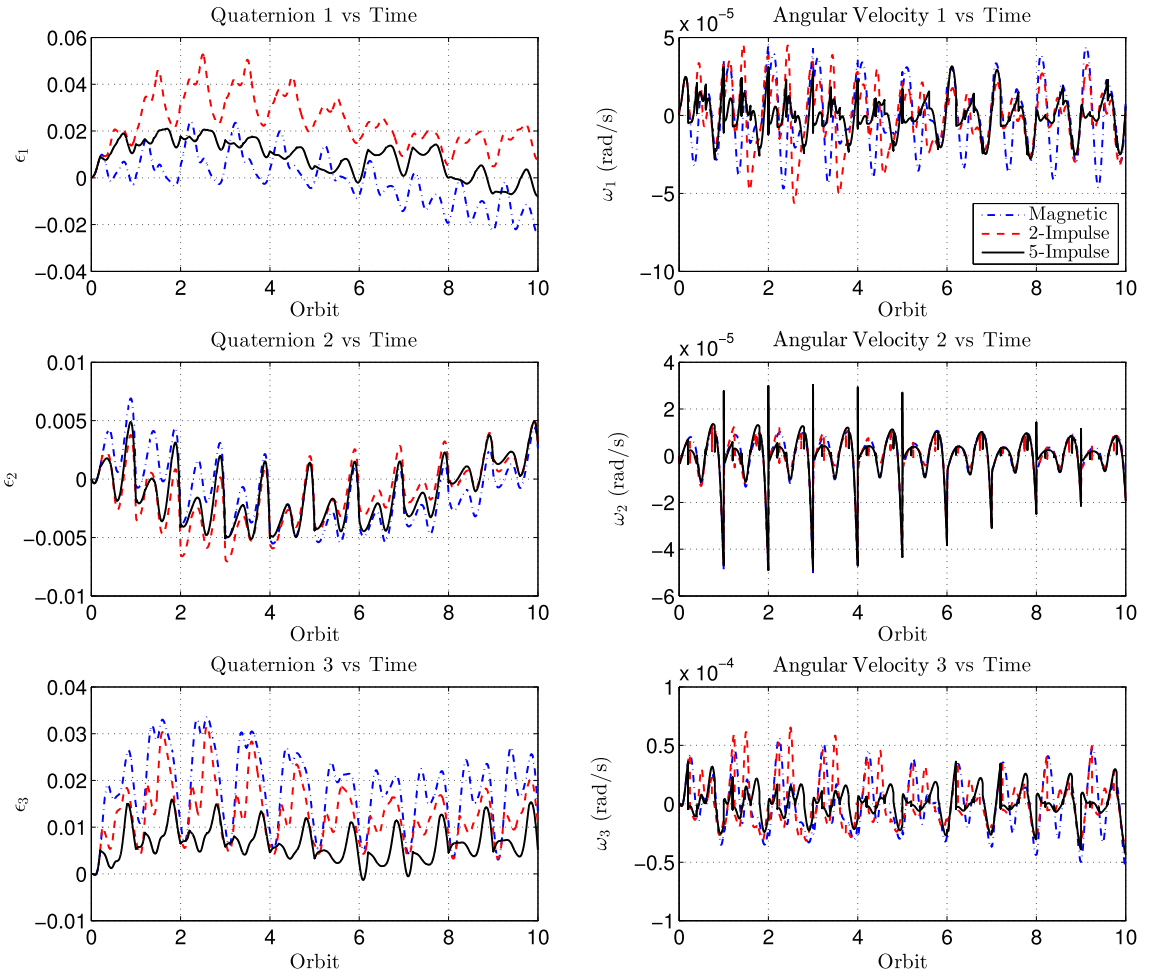

Fig. 6 Steady-state performance of constant-gain controller, with quaternions and angular velocity: passivity-based five-impulse hybrid (solid lines), two-impulse hybrid (dashed lines), and solely magnetic (dashed–dotted lines).

the relationship $\cos(\phi) = (\text{trace}\{\boldsymbol{C}_{BG}\} - 1)/2$ is used. For a measure of the impulsive torques, owing to their discrete nature, $\boldsymbol{v}$ is set to $\boldsymbol{\tau}_d \approx \boldsymbol{n}_k/h$ when $t_k \in [t, t+h)$ during the numerical integration (where the impulse is approximated with a rectangle of area $\boldsymbol{n}_k$ and finite width h) and to $\boldsymbol{\tau}_d = \boldsymbol{0}$ at all other time steps.

For the constant-gain controller represented by Table 1, the two-impulse controller's performance actually appears to be worse than that of the solely magnetic controller, although it does result in reduced angular velocities. By increasing the number of impulses using the five-impulse controller, however, in addition to ameliorated steady-state behavior (discussed in more detail in Sec. V.B), further improvements are seen in the norms reported in Table 1: most noticeably, that of the rotation angle is reduced by about 20 and 32% as compared to the solely magnetic and two-impulse cases, respectively. Table 1 also includes, as an external benchmark, the performance results using the proportional-derivative magnetic state feedback suggested in [28], with control input $\boldsymbol{u} = \boldsymbol{m} = \boldsymbol{b}_B^{\times}\boldsymbol{\nu}/|\boldsymbol{b}_G|^2$, where $\boldsymbol{\nu} = -(\gamma^2 k_p \boldsymbol{\epsilon} + \gamma k_v \boldsymbol{I}\boldsymbol{\omega})$. The scaling parameter and gains are set to $\gamma = 0.001$ and $k_p = k_v = 50$, which is consistent with [28] for the moment of inertia, and orbital parameters are the same. The passivity-based constant-gain controllers seem to perform better than the reference PD law in terms of all measures defined (disregarding the impulsive torques that are not used by the continuous-only schemes). Similar comments can be made about the dynamic compensator represented by Table 2: all passivity-based compensators perform better than the PD law used as a benchmark, and improvements are gained by adding an auxiliary impulsive mechanism with a sufficiently large number of thrusts.

B. Steady-State Behavior

Shown in Fig. 6 are the quaternions and angular velocities corresponding to simulations using the constant-gain controller; whereas depicted in Fig. 7 are those resulting from the use of the dynamic compensator, with the same spacecraft, orbit, and impulse patterns as those in Sec. V.A. In this section, however, the initial conditions are set to $\boldsymbol{\epsilon}_0 = 0$, $\eta_0 = 1$, and $\boldsymbol{\omega}_0 = [0 \quad 0 \quad 0]^{\intercal}$ rad/s. By eliminating the nonequilibrium initial conditions, the controllers are only influenced by the disturbances, so these results give an indication of their steady-state performance. For the constant-gain controller, based on Fig. 6, there seems to be no improvement resulting from the use of the two-impulse controller (dashed curves) compared to the solely magnetic one (dashed–dotted curves). However, increasing the number of impulses to five seems to reduce some of the errors. The large jumps in the angular velocities (especially in ω_2), shown in Fig. 6, occur every T and are caused by the resetting of the $\boldsymbol{P}(t)$ solution used for the plant's design. For practical applications, such sudden changes may not be desirable, motivating future work on the passivity-based design schemes in hopes of circumventing the resetting action used in Sec. IV.B. Alternatively, although all the dynamic compensators exhibit similar steady behaviors in Fig. 7, they seem to have reduced the undesirable ω_2 jumps to an extent, which seems logical owing to the filtering properties of compensators.

Table 3 lists the quantitative norms (defined identically to those in Tables 1 and 2) corresponding to the constant-gain controllers for these zero initial condition simulation cases. The numbers suggest that the two-impulse controller is, once again, worse than the purely magnetic one in terms of disturbance rejection. The five-impulse controller, however, improves all of the parameters, reducing the

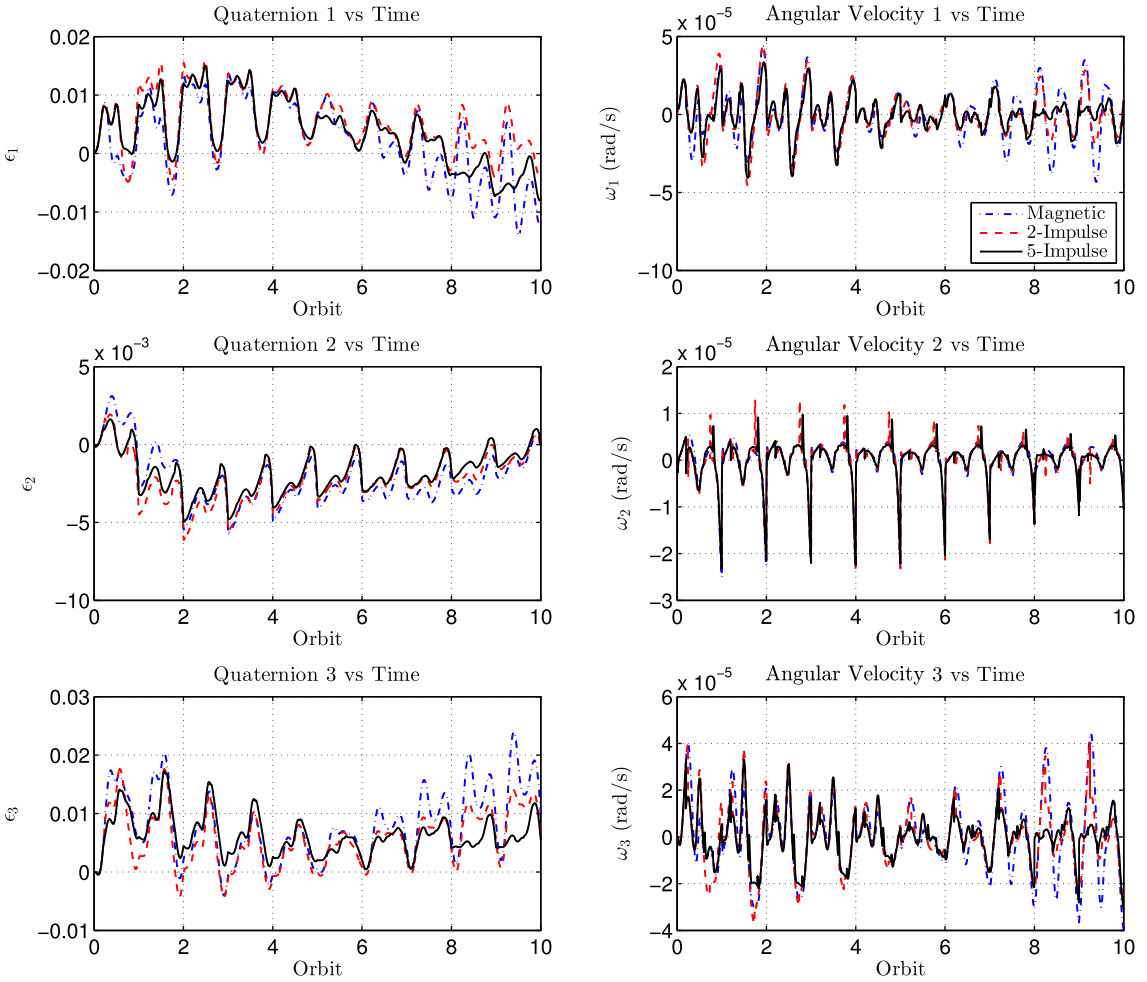

Fig. 7 Steady-state performance of dynamic compensator, with quaternions and angular velocity: passivity-based five-impulse hybrid (solid lines), two-impulse hybrid (dashed lines), and solely magnetic (dashed–dotted lines).

Table 3 Steady-state performance of reference PD (based on [28]) vs magnetic, two-impulse, and five-impulse constant-gain controllers over $10T$

Parameter	Description	Reference PD	Magnetic	Two-impulse	Five-impulse	Unit
E_{10T}	Electrical energy usage	8.39×10^{-5}	5.61×10^{-5}	7.36×10^{-5}	3.96×10^{-5}	MJ
$\|\boldsymbol{\tau}_c\|_{10T}$	Magnetic torque norm	5.28×10^{-6}	4.02×10^{-6}	4.26×10^{-6}	3.58×10^{-6}	N · m
$\|\boldsymbol{\tau}_d\|_{10T}$	Impulsive torque norm	0	0	5.59×10^{-5}	6.80×10^{-5}	N · m
$\|\boldsymbol{\omega}\|_{10T}$	Angular velocity norm	2.71×10^{-5}	3.27×10^{-5}	2.97×10^{-5}	1.98×10^{-5}	rad/s
$\|\boldsymbol{\phi}\|_{10T}$	Rotation angle norm	6.34×10^{-2}	4.55×10^{-2}	6.01×10^{-2}	2.78×10^{-2}	rad

Table 4 Steady-state performance of reference PD (based on [28]) vs magnetic, two-impulse, and five-impulse dynamic compensators over $10T$

Parameter	Description	Reference PD	Magnetic	Two-impulse	Five-impulse	Unit
E_{10T}	Electrical energy usage	8.39×10^{-5}	6.40×10^{-5}	7.21×10^{-5}	7.20×10^{-5}	MJ
$\|\boldsymbol{\tau}_c\|_{10T}$	Magnetic torque norm	5.28×10^{-6}	4.16×10^{-6}	4.37×10^{-6}	4.21×10^{-6}	N · m
$\|\boldsymbol{\tau}_d\|_{10T}$	Impulsive torque norm	0	0	1.68×10^{-5}	2.50×10^{-5}	N · m
$\|\boldsymbol{\omega}\|_{10T}$	Angular velocity norm	2.71×10^{-5}	2.26×10^{-5}	2.00×10^{-5}	1.57×10^{-5}	rad/s
$\|\boldsymbol{\phi}\|_{10T}$	Rotation angle norm	6.34×10^{-2}	2.49×10^{-2}	2.14×10^{-2}	2.00×10^{-2}	rad

magnetic torques by 30% compared to the solely magnetic case, as well as exhibiting a significant 40% decrease in both rotation angles and angular velocities. Once again, the passivity-based constant-gain controllers have generally better performance than the reference PD law, other than in terms of angular velocity, where the latter performs better than the passive magnetic and two-impulse controllers.

Presented in Table 4 are the steady-state performance norms computed for the passivity-based dynamic compensators. In general, the changes resulting from incorporating the impulses are not as pronounced as those in Table 3 for the constant-gain controllers. Unlike the two-impulse constant-gain controller, however, the two-impulse dynamic compensator does exhibit improved attitude and angular velocity compared to the corresponding solely magnetic controller, but at the cost of larger energy consumption. Similar comments hold for the five-impulse controller, which causes about 30 and 20% decreases in the angular velocities and rotation angles

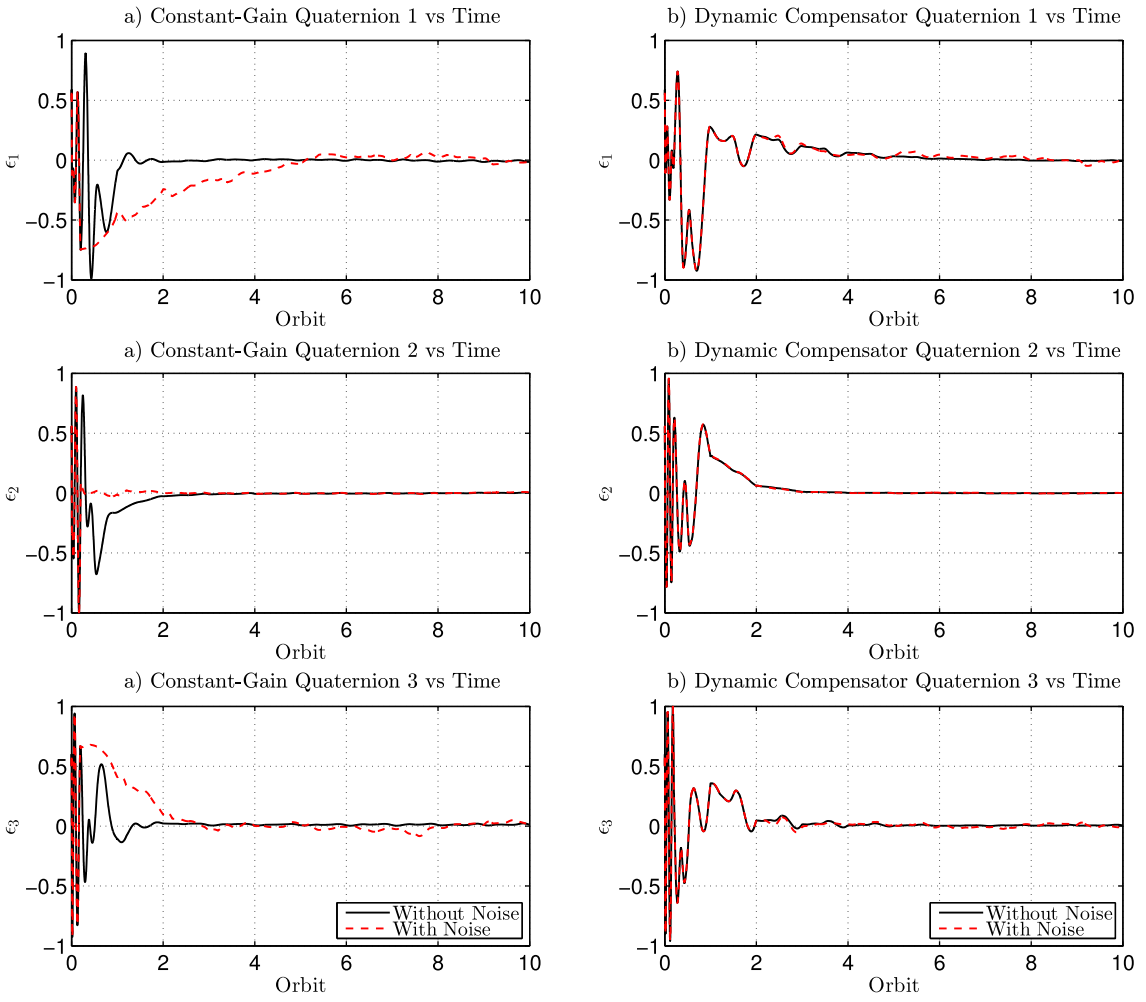

Fig. 8 Attitude performance of five-impulse a) constant-gain controller and b) dynamic compensator: without sensor noise (solid lines) and with sensor noise (dashed lines).

Table 5 Measurement noise effects on five-impulse constant-gain controller and dynamic compensator over $10T$

Parameter	Description	Constant (no noise)	Constant (noise)	Dynamic (no noise)	Dynamic (noise)	Unit
E_{10T}	Electrical energy usage	2.36×10^{1}	2.36×10^{1}	2.61×10^{1}	2.61×10^{1}	MJ
$\|\boldsymbol{\tau}_c\|_{10T}$	Magnetic torque norm	1.85×10^{-3}	1.85×10^{-3}	1.90×10^{-3}	1.90×10^{-3}	N · m
$\|\boldsymbol{\tau}_d\|_{10T}$	Impulsive torque norm	2.12×10^{-3}	5.82×10^{-3}	3.98×10^{-3}	3.97×10^{-3}	N · m
$\|\boldsymbol{\omega}\|_{10T}$	Angular velocity norm	4.59×10^{-3}	4.32×10^{-3}	4.65×10^{-3}	4.65×10^{-3}	rad/s
$\|\boldsymbol{\phi}\|_{10T}$	Rotation angle norm	6.22×10^{-1}	8.75×10^{-1}	6.90×10^{-1}	6.93×10^{-1}	rad

(compare to the 12 and 14% reductions obtained by the constant-gain five-impulse controller), respectively, but also consumes about 12% more energy. The reader is also reminded that all of the passivity-based controllers are guaranteed to satisfy (via their plant output design in Sec. IV.B and controller designs in Secs IV.C and IV.D) the hybrid (algebraic) KYP conditions outlined in Theorems 2.3 and 2.4, hence establishing the system's stability. This, in itself, is an advantage over similar (but not necessarily passive) attitude controllers.

C. Measurement Noise Effects

The attitude and rate measurements obtained and used for feedback control are never perfect, and there is always at least some unpredictable sensor noise present, the mean magnitude of which depends on the types of the sensors being used. To test the influence of measurement noise on the performance of the proposed passivity-based hybrid controllers, the state vector $\boldsymbol{x}(t)$ consisting of the direct attitude (converted to quaternions) and rate measurements is perturbed by a randomly generated zero-mean Gaussian white noise vector. Specifically, following the approach suggested in ([41] section 25.1.2), MATLAB's built-in random number generator $randn()$ is used to produce a vector of random numbers [namely, $\boldsymbol{\rho} \sim \mathcal{N}(\mathbf{0}, \mathbf{1}) \in \mathbb{R}^{6\times 1}$]; and the noise vectors to be added to the states are set to $\boldsymbol{E}\sqrt{\boldsymbol{\Lambda}}\boldsymbol{\rho}$, where $\boldsymbol{E}$ and $\boldsymbol{\Lambda}$ are obtained by diagonalizing the covariance matrix of the noise distribution as $\boldsymbol{\Sigma} = \boldsymbol{E}\boldsymbol{\Lambda}\boldsymbol{E}^{\intercal}$. This matrix is assumed to be constant, and it is set to $\boldsymbol{\Sigma} = \text{blockdiag}\{\sigma_\epsilon^2 \mathbf{1}_{3\times 3}, \sigma_\omega^2 \mathbf{1}_{3\times 3}\}$.

For the results reported in this section, the variance parameters associated with the attitude and rate measurements are set to $\sigma_\epsilon^2 = 5 \times 10^{-11}$ and $\sigma_\omega^2 = 5 \times 10^{-9}$, respectively, resulting in mean values of around 1.5×10^{-5} and 1.5×10^{-4} rad/s perturbations in $\boldsymbol{\epsilon}$ and $\boldsymbol{\omega}$, respectively. These are relatively large noises to consider for most spacecraft, so the resulting effects should be viewed as somewhat exaggerated.

Figures 8a and 8b compare the attitude control performance of the constant-gain controller and the dynamic compensator, respectively, with (dashed) and without (solid) the presence of measurement noise. Table 5 lists the performance parameters computed for each case over 10 orbits. The same design parameters as those in Sec. V.A are used, with the five-impulse case of both controllers selected. The same initial conditions as those in Sec. V.A are used: $\boldsymbol{\epsilon}_0 = [0.50 \quad 0.50 \quad 0.50]^{\intercal}$, $\eta_0 = 0.50$, and $\boldsymbol{\omega}_0 = [0.10 \quad 0.10 \quad 0.10]^{\intercal}$ rad/s.

As is evident from both Fig. 8 and Table 5, the dynamic compensator is much more immune to erroneous state knowledge, and it is thus expected to perform better than the constant-gain controller when significant sensor noise is anticipated. For example, when noise is added, the constant-gain controller uses about 175% more impulsive torque and results in a 40% increase in the rotation angles, whereas these numbers barely change for the dynamic compensator. Once again, this improved performance can be attributed to the dynamic compensator's filtering nature, and it provides another reason for why one should consider choosing the passivity-based compensator over the constant-gain controller, despite the former's significantly more complicated design procedure.

VI. Conclusions

Novel passivity-based attitude control schemes using magnetic torquers and impulsive thrusters in tandem have been presented. Hybrid (continuous/impulsive) controllers were developed by designing the output dynamics that artificially modify the plant's full state measurement in a manner that guarantees its hybrid passivity in a linearized sense. To this end, a set of hybrid extended KYP conditions is used while evoking a hybrid extension of the passivity theorem to stabilize the system using input strictly passive negative feedback control. Two designs were proposed for an input strictly passive controller: a constant-gain proportional controller, and a dynamic compensator that makes use of a set of hybrid algebraic KYP conditions to guarantee input strict passivity. Improvements in terms of controllability and gain limitation were expected as a result of using an auxiliary impulsive thrust mechanism, and thanks to the passivity-based approach, the controllers were anticipated to have good robustness and physically intuitive stability properties. In addition, the filtering properties of the dynamic compensator were expected and shown to result in improved sensor noise rejection. Numerical simulation results showed the functionality of all types of passivity-based controllers used, as well as transient and steady-state performance improvements as a result of adding an impulsive mechanism with a sufficient number of impulses. Further performance improvements, especially in the presence of sensor noise, were achieved by using a dynamic compensator instead of constant gains.

Appendix: Proofs of Auxiliary Theorems and Lemmas

Proof of Lemma 2.1: Consider the vector $\alpha\boldsymbol{v} + \beta\boldsymbol{w}$, with arbitrary scalars α and β, for which

$$(\|\alpha\boldsymbol{v} + \beta\boldsymbol{w}\|^h)^2 = \int_0^\infty (\alpha\boldsymbol{v}_c + \beta\boldsymbol{w}_c)^{\intercal}(\alpha\boldsymbol{v}_c + \beta\boldsymbol{w}_c)\,\mathrm{d}t + \sum_{k=1}^{\infty} (\alpha\boldsymbol{v}_d + \beta\boldsymbol{w}_d)^{\intercal}(\alpha\boldsymbol{v}_d + \beta\boldsymbol{w}_d) \geqslant 0 \tag{A1}$$

because the inner product of a vector with itself is always nonnegative. The time or index dependence of all vectors is omitted for clarity. We observe that $\boldsymbol{v} = \mathbf{0}$ or $\boldsymbol{w} = \mathbf{0}$ would trivially satisfy Eq. (A1). Assuming $\boldsymbol{v} \neq \mathbf{0}$ and $\boldsymbol{w} \neq \mathbf{0}$, we let $\alpha = 1/\|\boldsymbol{v}\|^h$ and $\beta = -1/\|\boldsymbol{w}\|^h$ in Eq. (A1):

$$\begin{aligned} 0 \leqslant \int_0^\infty \left(\frac{\boldsymbol{v}_c}{||\boldsymbol{v}||^h} - \frac{\boldsymbol{w}_c}{||\boldsymbol{w}||^h}\right)^{\intercal}\left(\frac{\boldsymbol{v}_c}{||\boldsymbol{v}||^h} - \frac{\boldsymbol{w}_c}{||\boldsymbol{w}||^h}\right) dt + \sum_{k=1}^{\infty}\left(\frac{\boldsymbol{v}_d}{||\boldsymbol{v}||^h} - \frac{\boldsymbol{w}_d}{||\boldsymbol{w}||^h}\right)^{\intercal}\left(\frac{\boldsymbol{v}_d}{||\boldsymbol{v}||^h} - \frac{\boldsymbol{w}_d}{||\boldsymbol{w}||^h}\right) \\ = \left(\int_0^\infty \frac{\boldsymbol{v}_c^{\intercal}\boldsymbol{v}_c}{||\boldsymbol{v}||^{h2}}\,dt + \sum_{k=1}^{\infty}\frac{\boldsymbol{v}_d^{\intercal}\boldsymbol{v}_d}{||\boldsymbol{v}||^{h2}}\,dt\right)^{1} + \left(\int_0^\infty \frac{\boldsymbol{w}_c^{\intercal}\boldsymbol{w}_c}{||\boldsymbol{w}||^{h2}}\,dt + \sum_{k=1}^{\infty}\frac{\boldsymbol{w}_d^{\intercal}\boldsymbol{w}_d}{||\boldsymbol{w}||^{h2}}\,dt\right)^{1} \\ - 2\left(\int_0^\infty \frac{\boldsymbol{v}_c^{\intercal}\boldsymbol{w}_c}{||\boldsymbol{v}||^h \cdot ||\boldsymbol{w}||^h}\,dt + \sum_{k=1}^{\infty}\frac{\boldsymbol{v}_d^{\intercal}\boldsymbol{w}_d}{||\boldsymbol{v}||^h \cdot ||\boldsymbol{w}||^h}\,dt\right) \quad \Rightarrow \quad 0 \leqslant 1 - \frac{\langle \boldsymbol{v}|\boldsymbol{w}\rangle^h}{||\boldsymbol{v}||^h \cdot ||\boldsymbol{w}||^h} \end{aligned} \tag{A2}$$

and rearranging the result yields Eq. (3a), as required. An identical approach can be used for Eq. (3b). □

Proof Theorem 2.1: Consider an arbitrary time instance: $\hat{t} > 0$. The difference between the value of V evaluated at $t = \hat{t}$ and $t = 0$ can be interpreted as the total sum of the changes over the first and last intervals (that of $\hat{t}$) and the instantaneous changes at each impulse time:

$$\begin{aligned} V(\hat{t}) - V(0) &= V(\hat{t}) + \sum_{k=1}^{\hat{N}-1}(-V(t_k^+) + V(t_k^+) - V(t_k^-) + V(t_k^-)) - V(0) \\ &= (V(\hat{t}) - V(t_{\hat{N}-1}^+)) + (V(t_{\hat{N}-1}^-) - V(t_{\hat{N}-2}^+)) + \cdots \\ &\quad + (V(t_1^-) - V(0)) + \sum_{k=1}^{\hat{N}-1}(V(t_k^+) - V(t_k^-)) \end{aligned} \tag{A3}$$

where $\hat{N} - 1$ indicates the number of impulses before $\hat{t}$, i.e., $t_{\hat{N}-1} < \hat{t} < t_{\hat{N}}$.

Substituting the conditions of Eq. (6) into Eq. (A3) yields the following:

$$\begin{aligned} V(\hat{t}) - V(0) \leqslant & \int_{t_{\hat{N}-1}^+}^{\hat{t}} \boldsymbol{y}_c^{\mathrm{T}} \boldsymbol{u}_c \, \mathrm{d}\tau + \int_{t_{\hat{N}-2}^+}^{t_{\hat{N}-1}^-} \boldsymbol{y}_c^{\mathrm{T}} \boldsymbol{u}_c \, \mathrm{d}\tau + \cdots \\ & + \int_0^{t_1^-} \boldsymbol{y}_c^{\mathrm{T}}(\tau) \boldsymbol{u}_c(\tau) \, \mathrm{d}\tau + \sum_{k=1}^{\hat{N}-1} \boldsymbol{y}_{dk}^{\mathrm{T}} \boldsymbol{u}_{dk} \end{aligned} \tag{A4}$$

where the τ dependence of the integrands is omitted. Lastly, because $\boldsymbol{y}_c^{\mathrm{T}} \boldsymbol{u}_c$ would have zero area at each point $t = t_k$, these points can also be included to obtain, upon evoking the condition $V(\hat{t}) \geqslant 0$,

$$-V(0) \leqslant \int_0^{\hat{t}} \boldsymbol{y}_c^{\mathrm{T}}(\tau) \boldsymbol{u}_c(\tau) \, \mathrm{d}\tau + \sum_{k=1}^{\hat{N}-1} \boldsymbol{y}_{dk}^{\mathrm{T}} \boldsymbol{u}_{dk} = \langle \boldsymbol{y} | \boldsymbol{u} \rangle_{\hat{t}}^h \tag{A5}$$

which establishes the passivity of the system $\boldsymbol{y} = \mathscr{G}\boldsymbol{u}$, with $\beta = -V(0) \leqslant 0$ as in Eq. (4) of Definition 2.4.

Similarly, substituting the conditions of Eq. (7) into Eq. (A3) produces

$$\begin{aligned} V(\hat{t}) - V(0) \leqslant & \int_{t_{\hat{N}-1}^+}^{\hat{t}} \boldsymbol{y}_c^{\mathrm{T}} \boldsymbol{u}_c \, \mathrm{d}\tau - \epsilon_{c(\hat{N}-1)} \int_{t_{\hat{N}-1}^+}^{\hat{t}} \boldsymbol{u}_c^{\mathrm{T}} \boldsymbol{u}_c \, \mathrm{d}\tau \\ & + \int_{t_{\hat{N}-2}^+}^{t_{\hat{N}-1}^-} \boldsymbol{y}_c^{\mathrm{T}} \boldsymbol{u}_c \, \mathrm{d}\tau - \epsilon_{c(\hat{N}-2)} \int_{t_{\hat{N}-2}^+}^{t_{\hat{N}-1}^-} \boldsymbol{u}_c^{\mathrm{T}} \boldsymbol{u}_c \, \mathrm{d}\tau \\ & + \cdots + \int_0^{t_1^-} \boldsymbol{y}_c^{\mathrm{T}} \boldsymbol{u}_c \, \mathrm{d}\tau - \epsilon_{c0} \int_0^{t_1^-} \boldsymbol{u}_c^{\mathrm{T}} \boldsymbol{u}_c \, \mathrm{d}\tau + \sum_{k=1}^{\hat{N}-1} \boldsymbol{y}_{dk}^{\mathrm{T}} \boldsymbol{u}_{dk} \\ & - \sum_{k=1}^{\hat{N}-1} \epsilon_{dk} \boldsymbol{u}_{dk}^{\mathrm{T}} \boldsymbol{u}_{dk} \end{aligned} \tag{A6}$$

where the τ dependence of the integrands is omitted. After rearranging and using the same argument as that for Eq. (A5), one obtains the following:

$$\begin{aligned} -V(0) + \sum_{\kappa=0}^{\hat{N}-1} \epsilon_{c\kappa} \int_{t_\kappa^+}^{t_{\kappa+1}^-} \boldsymbol{u}_c^{\mathrm{T}}(\tau) \boldsymbol{u}_c(\tau) \, \mathrm{d}\tau + \sum_{k=1}^{\hat{N}-1} \epsilon_{dk} \boldsymbol{u}_{dk}^{\mathrm{T}} \boldsymbol{u}_{dk} \leqslant \int_0^{\hat{t}} \boldsymbol{y}_c^{\mathrm{T}}(\tau) \boldsymbol{u}_c(\tau) \, \mathrm{d}\tau \\ + \sum_{k=1}^{\hat{N}-1} \boldsymbol{y}_{dk}^{\mathrm{T}} \boldsymbol{u}_{dk} = \langle \boldsymbol{y} | \boldsymbol{u} \rangle_{\hat{t}}^h \end{aligned} \tag{A7}$$

Finally, defining $\epsilon = \min\{\{\epsilon_{c\kappa}\} \cup \{\epsilon_{dk}\}\} > 0$ (i.e., the smallest of all ϵ_c and ϵ_d; all of which are positive), Eq. (A7) implies the following:

$$\begin{aligned} -V(0) + \epsilon(\|\boldsymbol{u}\|_{\hat{t}}^h)^2 = -V(0) + \epsilon \Bigg(& \int_0^{\hat{t}} \boldsymbol{u}_c^{\mathrm{T}}(\tau) \boldsymbol{u}_c(\tau) \, \mathrm{d}\tau \\ & + \sum_{k=1}^{\hat{N}-1} \boldsymbol{u}_{dk}^{\mathrm{T}} \boldsymbol{u}_{dk} \Bigg) \leqslant \langle \boldsymbol{y} | \boldsymbol{u} \rangle_{\hat{t}}^h \end{aligned} \tag{A8}$$

which establishes the input strict passivity of the system $\boldsymbol{y} = \mathscr{G}\boldsymbol{u}$, with $\beta = -V(0) \leqslant 0$ as in Eq. (5) of Definition 2.4. □

References

[1] Desoer, C. A., and Vidyasagar, M., *Feedback Systems: Input-Output Properties*, Academic Press Inc., London, 1963, pp. 181–182.

[2] Ortega, R., and García-Canseco, E., "Interconnection and Damping Assignment Passivity-Based Control: A Survey," *European Journal of Control*, Vol. 10, No. 5, 2004, pp. 432–450. doi:10.3166/ejc.10.432-450

[3] Popov, V. M., "Absolute Stability of Nonlinear Systems of Automatic Control," *Automation and Remote Control*, Vol. 22, No. 8, Aug. 1961, pp. 961–979.

[4] Yakubovich, V. A., "The Solution of Certain Matrix Inequalities in Automatic Control Theory," *Soviet Mathematics*, Vol. 3, No. 2, 1962, pp. 620–623.

[5] Kalman, R. E., "Lyapunov Functions for the Problem of Lur'e in Automatic Control," *Proceedings of the National Academy of Sciences of the USA*, Vol. 49, No. 2, Feb. 1963, pp. 201–205.

[6] Anderson, B. D. O., "A System Theory Criterion for Positive Real Matrices," *SIAM Journal on Control*, Vol. 5, No. 2, May 1967, pp. 171–182. doi:10.1137/0305011

[7] Willems, J. C., "Dissipative Dynamical Systems, Part I: General Theory," *Archive for Rational Mechanics and Analysis*, Vol. 45, No. 5, Jan. 1972, pp. 321–351. doi:10.1007/BF00276493

[8] Willems, J. C., "Dissipative Dynamical Systems, Part II: Linear Systems with Quadratic Supply Rates," *Archive for Rational Mechanics and Analysis*, Vol. 45, No. 5, Jan. 1972, pp. 352–393. doi:10.1007/BF00276494

[9] Hill, D., and Moylan, P., "The Stability of Nonlinear Dissipative Systems," *IEEE Transactions on Automatic Control*, Vol. 21, No. 5, Oct. 1976, pp. 708–711. doi:10.1109/TAC.1976.1101352

[10] Haddad, W. M., Chellaboina, V., and Kablar, N. A., "Non-Linear Impulsive Dynamical Systems. Part I: Stability and Dissipativity," *International Journal of Control*, Vol. 74, No. 17, 2001, pp. 1631–1658. doi:10.1080/00207170110081705

[11] Haddad, W. M., Chellaboina, V., and Kablar, N. A., "Non-Linear Impulsive Dynamical Systems. Part II: Stability of Feedback Interconnections and Optimality," *International Journal of Control*, Vol. 74, No. 17, 2001, pp. 1659–1677. doi:10.1080/00207170110080959

[12] Žefran, M., Bullo, F., and Stein, M., "A Notion of Passivity for Hybrid Systems," *Proceedings of the 40th IEEE Conference on Decision and Control*, Vol. 1, IEEE, Piscataway, NJ, Dec. 2001, pp. 768–773. doi:10.1109/.2001.980199

[13] Lin, W., "Feedback Stabilization of General Nonlinear Control Systems: A Passive System Approach," *Systems and Control Letters*, Vol. 25, No. 1, May 1995, pp. 41–52. doi:10.1016/0167-6911(94)00056-2

[14] Kelkar, A. G., and Joshi, S. M., "Passivity-Based Robust Control with Application to Benchmark Active Controls Technology Wing," *Journal of Guidance, Control, and Dynamics*, Vol. 23, No. 5, Sept.–Oct. 2000, pp. 938–947. doi:10.2514/2.4636

[15] Naldi, R., and Sanfelice, R. G., "Passivity-Based Control for Hybrid Systems with Applications to Mechanical Systems Exhibiting Impacts," *Automatica*, Vol. 49, No. 5, May 2013, pp. 1104–1116. doi:10.1016/j.automatica.2013.01.018

[16] Forbes, J. R., and Damaren, C. J., "Linear Time-Varying Passivity-Based Attitude Control Employing Magnetic and Mechanical Actuation," *Journal of Guidance, Control, and Dynamics*, Vol. 34, No. 5, Sept.–Oct. 2011, pp. 1363–1372. doi:10.2514/1.51899

[17] de Ruiter, A. H. J., "Some Applications of Passivity-Based Control and Invariance Principles," *IET Control Theory and Applications*, Vol. 7, No. 7, May 2013, pp. 1039–1048. doi:10.1049/iet-cta.2012.0691

[18] Benhabib, R. J., Iwens, R. P., and Jackson, R. L., "Stability of Large Space Structure Control Systems Using Positivity Concepts," *Journal of Guidance, Control, and Dynamics*, Vol. 4, No. 5, Sept.–Oct. 1981, pp. 487–494.
doi:10.2514/3.56100

[19] Wertz, J. R., *Spacecraft Attitude Determination and Control*, D. Reidel Publishing, Dordrecht, The Netherlands, 1978.

[20] White, J. S., Shigemoto, F. H., and Bourquin, K., "Satellite Attitude Control Utilizing the Earth's Magnetic Field," NASA TN-D10-68 A-474, Aug. 1961.

[21] Wiśniewski, R., and Blanke, M., "Fully Magnetic Attitude Control for Spacecraft Subject to Gravity Gradient," *Automatica*, Vol. 35, No. 7, July 1999, pp. 1201–1214.
doi:10.1016/S0005-1098(99)00021-7

[22] Wiśniewski, R., "Linear Time-Varying Approach to Satellite Attitude Control Using Only Electromagnetic Actuation," *Journal of Guidance, Control, and Dynamics*, Vol. 23, No. 4, July–Aug. 2000, pp. 640–647.
doi:10.2514/2.4609

[23] Damaren, C. J., "Comments on 'Fully Magnetic Attitude Control for Spacecraft Subject to Gravity Gradient'," *Automatica*, Vol. 38, No. 12, Dec. 2002, Paper 2189.
doi:10.1016/S0005-1098(02)00146-2

[24] Cubas, J., Farrahi, A., and Pindado, S., "Magnetic Attitude Control for Satellites in Polar or Sun-Synchronous Orbits," *Journal of Guidance, Control, and Dynamics*, Vol. 38, No. 10, Oct. 2015, pp. 1947–1958.
doi:10.2514/1.G000751

[25] Stickler, A. C., and Alfriend, K. T., "Elementary Magnetic Attitude Control System," *Journal of Spacecraft and Rockets*, Vol. 13, No. 5, May 1976, pp. 282–287.
doi:10.2514/3.57089

[26] Silani, E., and Lovera, M., "Magnetic Spacecraft Attitude Control: A Survey and Some New Results," *Control Engineering Practice*, Vol. 13, No. 3, Mar. 2005, pp. 357–371.
doi:10.1016/j.conengprac.2003.12.017

[27] Martel, F., Pal, P. K., and Psiaki, M., "Active Magnetic Control System for Gravity Gradient Stabilized Spacecraft," *Proceedings of the 2nd Annual AIAA/USU Conference on Small Satellites*, Logan, UT, Sept. 1988.

[28] Lovera, M., and Astolfi, A., "Spacecraft Attitude Control Using Magnetic Actuators," *Automatica*, Vol. 40, No. 8, Aug. 2004, pp. 1405–1414.
doi:10.1016/j.automatica.2004.02.022

[29] Camillo, P. J., and Markley, F. L., "Orbit-Averaged Behavior of Magnetic Control Laws for Momentum Unloading," *Journal of Guidance, Control, and Dynamics*, Vol. 3, No. 6, Nov.–Dec. 1980, pp. 563–568.
doi:10.2514/3.19725

[30] Arduini, C., and Baiocco, P., "Active Magnetic Damping Attitude Control for Gravity Gradient Stabilized Spacecraft," *Journal of Guidance, Control, and Dynamics*, Vol. 20, No. 1, Jan.–Feb. 1997, pp. 117–122.
doi:10.2514/2.4003

[31] Psiaki, M. L., "Magnetic Torquer Attitude Control via Asymptotic Periodic Linear Quadratic Regulation," *Journal of Guidance, Control, and Dynamics*, Vol. 24, No. 2, March–April 2001, pp. 386–394.
doi:10.2514/2.4723

[32] Lovera, M., de Marchi, E., and Bittanti, S., "Periodic Attitude Control Techniques for Small Satellites with Magnetic Actuators," *IEEE Transactions on Control Systems Technology*, Vol. 10, No. 1, Jan. 2002, pp. 90–95.
doi:10.1109/87.974341

[33] Pittelkau, M. E., "Optimal Periodic Control for Spacecraft Pointing and Attitude Determination," *Journal of Guidance, Control, and Dynamics*, Vol. 16, No. 6, Nov.–Dec. 1993, pp. 1078–1084.
doi:10.2514/3.21130

[34] Pulecchi, T., Lovera, M., and Varga, A., "Optimal Discrete-Time Design of Three-Axis Magnetic Attitude Control Laws," *IEEE Transactions on Control Systems Technology*, Vol. 18, No. 3, May 2010, pp. 714–722.
doi:10.1109/TCST.2009.2024757

[35] Lovera, M., and Astolfi, A., "Global Magnetic Attitude Control of Inertially Pointing Spacecraft," *Journal of Guidance, Control, and Dynamics*, Vol. 28, No. 5, Sept.–Oct. 2005, pp. 1065–1072.
doi:10.2514/1.11844

[36] Vatankhahghadim, B., and Damaren, C. J., "Optimal Combination of Magnetic Attitude Control with Impulsive Thrusting," *Journal of Guidance, Control, and Dynamics*, Vol. 39, No. 10, Oct. 2016, pp. 2391–2398.
doi:10.2514/1.G001664

[37] Brogliato, B., Lozano, R., Maschke, B., and Egeland, O., *Dissipative Systems Analysis and Control: Theory and Applications*, Springer, London, 2007, p. 2.

[38] Byrnes, C. I., and Lin, W., "Losslessness, Feedback Equivalence, and the Global Stabilization of Discrete-Time Nonlinear Systems," *IEEE Transactions of Automatic Control*, Vol. 39, No. 1, Jan. 1994, pp. 83–98.
doi:10.1109/9.273341

[39] Lin, W., and Byrnes, C. I., "KYP Lemma, State Feedback and Dynamic Output Feedback in Discrete-Time Bilinear Systems," *Systems and Control Letter*, Vol. 23, No. 2, Aug. 1994, pp. 127–136.
doi:10.1016/0167-6911(94)90042-6

[40] Hughes, P. C., *Spacecraft Attitude Dynamics*, Wiley, New York, 1986.

[41] de Ruiter, A. H. J., Damaren, C. J., and Forbes, J. R., *Spacecraft Dynamics and Control: An Introduction*, Wiley, Hoboken, NJ, 2013.